




Development of a ternary cyclodextrin–arginine–ciprofloxacin antimicrobial complex with enhanced stability

Marija Vukomanovic ^{1,2}✉, Lea Gazvoda^{1,2}, Mario Kurtjak¹, Jitka Hrescak³, Blaž Jaklic^{1,2}, Laura Moya-Andérico⁴, Maria del Mar Cendra ⁴ & Eduard Torrents ^{4,5}✉

Designing useful functionalities in clinically validated, old antibiotics holds promise to provide the most economical solution for the global lack of effective antibiotics, as undoubtedly a serious health threat. Here we show that using the surface chemistry of the cyclodextrin (β CD) cycle and arginine (arg) as a linker, provides more stable ternary antibiotic complex (β CD-arg-cpx). In contrast to classical less stable inclusion complexes, which only modify antibiotic solubility, here-presented ternary complex is more stable and controls drug release. The components of the complex intensify interactions with bacterial membranes and increase the drug's availability inside bacterial cells, thereby improving its antimicrobial efficacy and safety profile. Multifunctional antibiotics, formulated as drug delivery systems per se, that take the drug to the site of action, maximize its efficacy, and provide optical detectability are envisaged as the future in fighting against infections. Their role as a tool against multi-resistant strains remains as interesting challenge open for further research.

¹Advanced Materials Department, Institute Jozef Stefan, Jamova 39, Ljubljana, Slovenia. ²International Postgraduate School of Jozef Stefan, Jamova 39, Ljubljana, Slovenia. ³Center for Electronic Microscopy and Microanalysis (CEMM), Institute Jozef Stefan, Jamova 39, Ljubljana, Slovenia. ⁴Bacterial Infections: Antimicrobial Therapies, Institute for Bioengineering of Catalonia (IBEC), The Institute of Science and Technology, Baldri Reixac 15-21, 08028 Barcelona, Spain. ⁵Microbiology Section, Department of Genetics, Microbiology and Statistics, Faculty of Biology, University of Barcelona, 643 Diagonal Ave., 08028 Barcelona, Spain. ✉email: marija.vukomanovic@ijs.si; etorrents@ibecbarcelona.eu

The dwindling of effective antimicrobials poses a very serious threat to global health in the modern world, as the World Health Organization recently pointed out¹. Only a few novel antibiotics have reached the market in the last few decades, and no completely new class of antibiotics has been discovered since 1980². With enormous costs and unpredictable and short-term benefits, the discovery of new antibiotics is not a major priority for the pharmaceutical industry^{2,3}. Repurposing, reprofiling, or reusing clinically approved medicines has important advantages in time and cost over discovering new drug candidates, especially in emerging situations such as pandemics^{4,5}. The critical benefits are a predictable safety profile, previous knowledge on manufacturing procedures, established testing protocols, more straightforward regulatory requirements, and shorter bench-to-market periods, among many others^{6,7}. Therefore, it is not surprising that approximately one-third of all approved medicines in the last decade have been repurposed old drugs, which account for 25% of the revenue in the pharmaceutical industry^{7,8}. Much of the effort in the current preclinical antibiotic pipeline is focused on modifying old antibiotics to increase their efficacy, particularly in synergy with other drugs or auxiliary nondrug components^{9,10}. The main scientific challenges in achieving this are the limited penetration, efflux, and toxicity associated with high-dose treatment^{9,10}.

A simple and very effective approach to redesigning old antibiotics includes the formation of instable complexes that modify properties such as solubility, stability, bioavailability, and permeability, thereby directly influencing their therapeutic outcome. In that context, cyclodextrins (CDs) are particularly applicable^{11,12}. With a truncated cone structure, they have a hydrophilic shell (with 7 primary groups oriented toward the narrow edge and 14 secondary sugar hydroxyl groups oriented toward the wider edge of the cone, in the case of β -CD) and a hydrophobic core (with a carbon backbone of 7 glucopyranose units that make up the structure of β -CD) available for interactions with drug molecules^{11,13,14}. Most commonly, antibiotics are formulated as inclusion complexes when the hydrophobic part of the drug interacts with the hydrophobic inner core area of the CD, which consequently increases its solubility by several times¹¹. This approach has been applied to various antibiotics (β -lactams, microlidols, fluoroquinolones, sulfonamides, tetracyclines, and aminoglycosides), and their minimal inhibitory concentrations (MICs) were reduced by factors from 2 to more than 100¹¹. It is an enthalpy-driven process, and the host-guest CD-drug complex is in equilibrium with the free drug without chemical bonding¹². This approach becomes even more effective if the CD excipient is combined with specially selected auxiliary components (such as hydrophilic polymers, amino acids, or hydroxyl acids) to form ternary complexes^{15–18}. The hydrophobic part of the drug forms a CD-drug inclusion complex, while the hydrophilic part simultaneously undergoes an acid-base reaction with the auxiliary component to form a salt.

A good example is arginine, a basic amino acid, which forms salts with acidic drugs (e.g., naproxen, zoloprofen, oxaprozin) complexed with CD^{16–18}. As a result, an important increase in the stability constant and complexation efficacy is obtained. Therefore, it is expected that combining an antibiotic with CD and arginine into a ternary complex might strongly influence its antimicrobial activity. However, only a few investigations of such complexes have been conducted thus far, among which a study on cefuroxime has shown drastically increased solubility after the formation of ternary complexes with CD and arginine¹⁹.

Instead of the less stable inclusion complexes usually formed to increase drug solubility, we designed a more stable antibiotic ternary β -cyclodextrin-arginine-ciprofloxacin (β CD-arg-cpx) complex, in which ciprofloxacin (cpx) is attached to the hydrophilic surface of β CD via an arginine (arg) linker. With this

approach, our goal was not simply increasing the solubility of the drug as usual. Here, our synthesized complex system is importantly more stable to control antibiotic release, enable enhanced interactions with the bacterial cell wall and membranes, and provide higher permeability and availability inside the bacteria, consequently improving the efficacy of antibacterial treatment. Along with improved antimicrobial efficacy, considerable improvement in the safety profile was demonstrated.

Results and discussion

CD complex structure and formation. The β CD-arg-cpx complex assembles into well-organized 3D structures (Fig. 1a) as a few micrometers long rods (Fig. 1b) with highly ordered, radial structures composed of laterally connected plates a few tens of nanometers thick (Fig. 1c). A closer look at the single plates and the associated electron diffraction pattern (Fig. 1d) reveals their single-crystalline nature. Morphologically, these assemblies differ from β CD-cpx, and β CD-arg complexes were detected as irregularly shaped, non-assembled particles (Fig. 1e–g).

Elemental mapping in a single rod β CD-arg-cpx complex (Fig. 2a₁) detected C (Fig. 2a₂), F (Fig. 2a₃), N (Fig. 2a₄) and O (Fig. 2a₅) elements homogeneously distributed along the large area of a crystal. Further surface composition XPS analysis was performed on cpx drug reference as well as on β CD-arg-cpx complex before and after soft etching with Ar⁺ ions. Since N is present both in antibiotic and arginine (not in CD), while F is present only in cpx, higher N/F ratio in a complex compare to cpx was due to arginine bonding. On the other hand, decreasing C/F and O/F ratios from surface to bulk of the β CD-arg-cpx complex confirmed β CD at the surface. As F- side of cpx is not included in complexation, the maximum at 687.5 eV in F1s spectrum (corresponding to C-F bonds)²⁰ remains unchanged for all three investigated systems (Fig. 2b₂). On the other hand, N1s (with two maxima at 401.1 eV and 399.7 eV, corresponding to C-N-C and C-NH bonds²⁰, Fig. 2b₄) reveals increased fraction of primarily amines in complex then in cpx free drug which is due to bonding of arginine part. Their increase is observed in bulk area of the complex. The C1s spectrum (with maxima at 287 eV, 285.8 eV and 284.8 eV corresponding to C=O, C-N and C-C, respectively)²⁰ and O1s (with maxima at 533.1 eV and 531.5 eV, corresponding to C-O and (C=O)-OH, respectively)²⁰ show decrease of intensities of maxima belonging to C-O and C-N groups in a complex compare to the free cpx reference which is due to their involvement in complexation.

The high-aspect-ratio β CD-arg-cpx complex assemblies are highly crystalline, as indicated by their sharp polycrystalline diffraction maxima (Supplementary Fig. 1a). The detected crystal structure is similar to that of the basic deprotonated cpx (as observed in ref.²¹), with shifted diffraction maxima and the appearance of new peaks. It also differs slightly from the structure detected for the β CD-NaOH-cpx complex (a reference precipitated by replacing arg with NaOH) and exactly matches the structure of arg-cpx (a reference corresponding to the ciprofloxacin-arginine salt) (Supplementary Fig. 1a), which results from the acid-basic reaction between cpx and arg, formation of the salt and its crystallization. In contrast, crystallization of the separated cpx and arg components within β CD-cpx and β CD-arg complex aggregates is low, giving low intensity and broad diffraction maxima (Supplementary Fig. 1a). Due to the absence of the assembly, the crystal order in these structures is notably decreased. Therefore, the crystalline part of β CD-arg-cpx consisted of arg-cpx salt with an amorphous β CD component associated at the crystal surface.

Large structural differences among the different types of complexes were observable particularly in their FTIR spectra

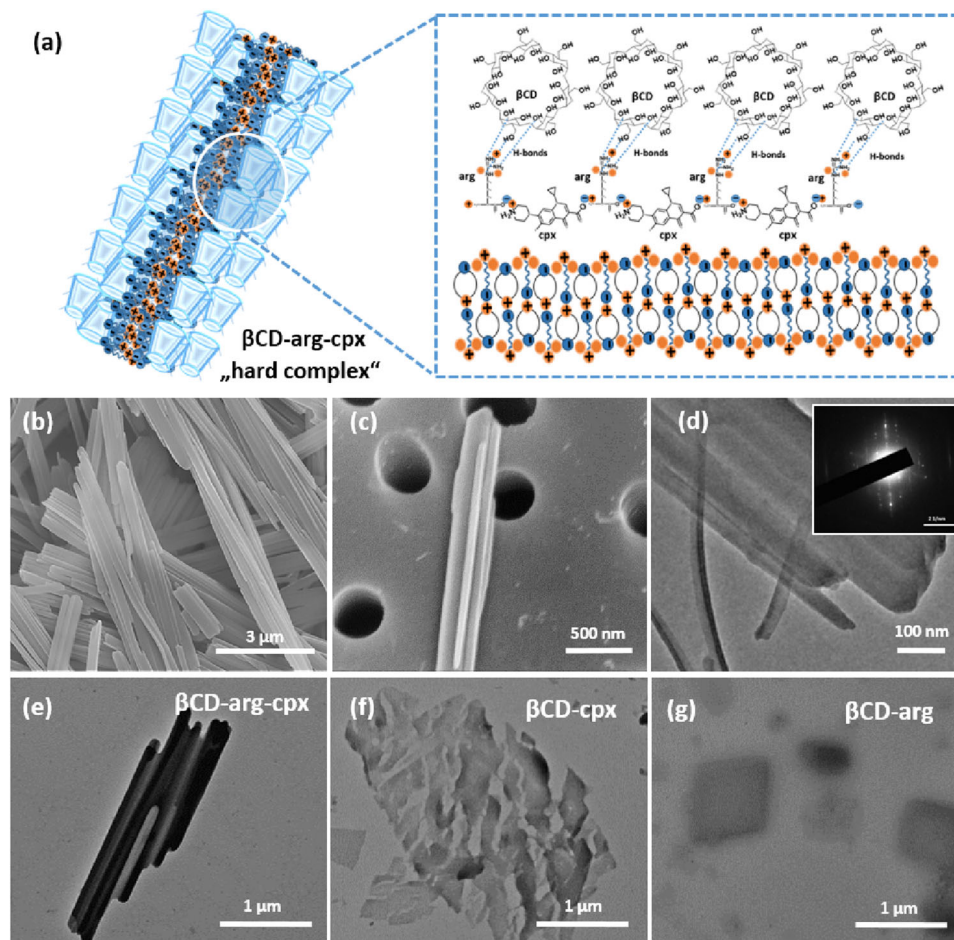


Fig. 1 Structural properties of more stable β CD-arg-cpx complex. Illustration of the structure with an arg-cpx crystalline core and β CD at the surface (a). SEM morphology showing long, aligned, rod-like structures of β CD-arg-cpx complex (b) with sharp, nanothick edges (c). Higher-magnification TEM image of the β CD-arg-cpx rods (d) and EDS pattern showing their crystalline nature (insert in (d)). TEM structures revealing differences among β CD-arg-cpx (e), β CD-cpx (f) and β CD-arg (g).

(Supplementary Fig. 1b). The FTIR spectrum of the inclusion β CD-arg complex (Supplementary Fig. 1b) showed typical β CD bands with broad O-H stretching at 3300 cm^{-1} and O-H bending at 1640 cm^{-1} , and C-H stretching at 2925 cm^{-1} , and ring vibration bands as asymmetrical C-O-C and C-C stretching at 1152 cm^{-1} , 1026 cm^{-1} , and 932 cm^{-1} ^{17,22,23}, and guanidine C-N stretching modes from arginine at 1554 cm^{-1} (more details in Supplementary Fig. 2)²⁴. The intensity of the O-H stretching and bending modes from β CD was altered in the β CD-arg spectrum, but no additional bands were observed (Supplementary Fig. 2). In the β CD-cpx complex, slight position shifts were observed for the bands corresponding to aromatic ring vibrations of cpx and β CD obtained due to the incorporation of the molecule inside the β CD cone, which is typical of inclusion complexes (Supplementary Fig. 3)^{25,26}. In addition, the carboxyl C=O vibrational band of cpx at 1708 cm^{-1} indicated a neutral molecular form^{25,26}. The β CD-cpx complex did not show any additional bands (Supplementary Fig. 3).

A completely different situation was observed for the β CD-arg-cpx complex (Supplementary Fig. 1b). The stretching carbonyl C=O vibration mode, detected at 1708 cm^{-1} in β CD-cpx and also in physical mixture of β CD, arg and cpx components, is missing in spectra of both complexes, β CD-arg-cpx and β CD-NaOH-cpx, while complexes' asymmetric carboxylate vibration (which was missing in case of physical mixture and β CD-cpx) appears at 1578 cm^{-1} both indicating zwitterion cpx forms within

the β CD-arg-cpx and β CD-NaOH-cpx (Supplementary Figs. 3 and S4). In contrast to the spectrum of the inclusion complex β CD-cpx and the spectrum of a physical mixture of components from the complex, in β CD-arg-cpx, the cpx O-H stretching vibration at 3526 cm^{-1} was missing, another indication of its deprotonated form within the complex. Moreover, typical vibrational bands observed in previous complexes appeared in the spectrum of β CD-arg-cpx with higher intensity, changed intensity ratios, and higher resolution, indicating an increase in the structural order and crystallinity (as observed to carbonyl group vibrations in formulations containing semicrystalline cpx)²⁶. Novel vibrational bands were detected, particularly in the fingerprint area (Supplementary Fig. 4), that did not belong to any of the separate components of the complex (separately and in their physical mixture) but were a consequence of the new complex structure. It was interesting to observe that most of the new bands obtained for β CD-arg-cpx were also detected in arg-cpx and β CD-NaOH-cpx, adjusted to the same pH by using arginine or NaOH, which additionally confirmed the similar structure of complexes formed using these two acidity modulators. However, the presence of arginine within β CD-arg-cpx affected the β CD cycle ring vibrations, observed as the absence of the β CD-typical vibrations at 1079 and 996 cm^{-1} and additional vibration freedom detected through the new band at 1178 cm^{-1} , which was not detected in β CD-NaOH-cpx. These new interactions within β CD-arg-cpx could be a source of better complex

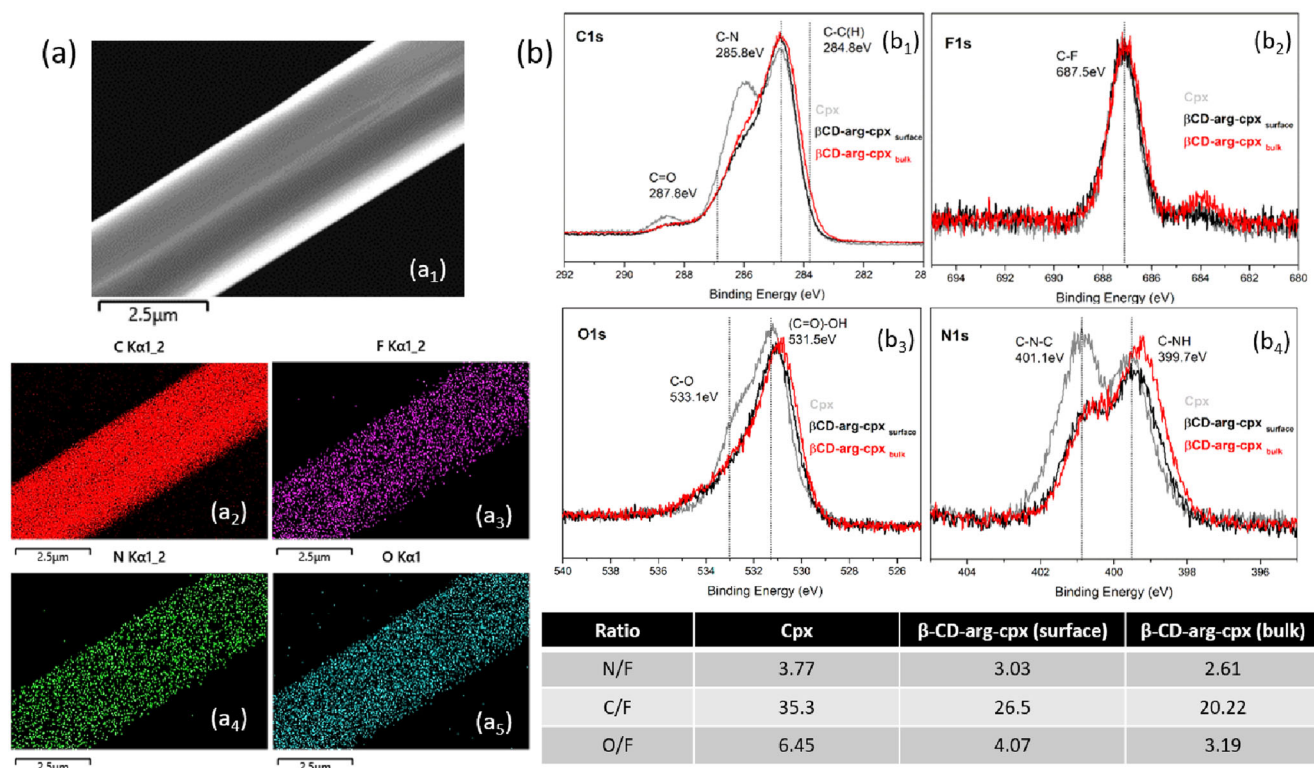


Fig. 2 Chemistry of the β CD-arg-cpx stable complex structure. STEM image (a_1) with elemental mapping analysis corresponding to carbon (C) (a_2), oxygen (O) (a_3), nitrogen (N) (a_4) and fluorine (F) (a_5); XPS analysis of the surface and bulk (obtained after soft etching) of the β CD-arg-cpx complex in comparison to pristine cpx reference- C1s (b_1), F1s (b_2), O1s (b_3) and N1s (b_4) high resolution spectra.

stability, which will be shown later. Investigations of the optical properties of the β CD- complexes enabled further insights into their structural characteristics. The fluorescence emission spectra of the β CD-arg-cpx and arg-cpx complexes (Supplementary Fig. 1c) showed a bathochromic shift when the β CD component was bonded to arg-cpx salt. A shift was observed in both cases when β CD was bonded to the β CD-arg-cpx or β CD-NaOH-cpx complex (Supplementary Fig. 1c). Indirectly, this observation confirmed the presence of this amorphous component on top of deprotonated cpx crystals (detected in XRD and further revealed in FTIR) and provided evidence of the bonding position. The observed fluorescence was assigned to the antibiotic molecule, with piperazinyl electron donor and 4-oxoquinoline-3-carboxylic acid electron acceptor groups²⁷. Similarly, in the present case, cpx is bonded via arg to β CD via a piperazinyl group with an electron donor nature. Bonding the cpx molecule over the arginine linker to β CD (or directly to the β CD molecule) limits its intramolecular motions and eliminates nonradiant relaxations, enabling fluorescence at the λ_{\max} shifted compare to free drug form.

Monitoring pH and zeta potential and replacing arg with NaOH as a pH modifier revealed critical steps toward complex formation (Fig. 3). Initially, the reaction mixture was pH 7.5, at which β CD has available OH groups, arg is in zwitterion form with a cationic charge at guanidine and deprotonated carboxyl groups, and cpx has a cationic amine on piperazinyl and deprotonated carboxyl groups (as illustrated in Fig. 3a). β CD-arg-Cpx complex formation starts with an acid-based reaction in which the carboxyl groups in arg interact with the cationic amine on the piperazinyl cpx side, forming an arg-cpx salt (Fig. 3b). The precipitation crystallization step enables the formation of long rod structures. The surface of the formed crystals has free guanidine groups available for bonding amorphous β CD components and assembling the final CD-arg-Cpx complex

(Fig. 3b). Amines in the guanidine functional group in arginine have a very high affinity for hydrogen bonding, with the possibility of forming up to five bonds involving both protonated and nonprotonated amines²⁸. Therefore, in the formed complex, arginine has the role of a linker, which uses cationic guanidine groups to bond β CD to the surface and ionic carboxyl groups to bond cpx. The zeta potential of β CD (initially at pH = 6) is changed after adding arginine (Table in Fig. 3), indicating interactions between cationic guanidine backbone groups and OH groups at the hydrophilic outer side of β CD.

The formed CD-arg-cpx complex structure appears as a shiny opal-white precipitate within two hours after mixing all the components. When β CD is mixed directly with cpx without adding arginine, the solution remains clear without any precipitation. Measuring the zeta potential of the lyophilized powder gives neutral values corresponding to nonstable β CD-cpx complex aggregates. As observed earlier, the β CD-cpx inclusion complex forms by incorporating hydrophobic 4-oxoquinoline-3-carboxylic acid moiety of the cpx molecule inside the hydrophobic cone of β CD²⁹. When the acidity of the initial reaction mixture was adjusted by using NaOH (instead of arginine), the precipitation of β CD-NaOH-cpx as an arg-free complex was much slower and did not take place after two hours of mixing, as in the case of β CD-arg-cpx (illustrated in photos in Fig. 3a), but was delayed during the following 24 h. β CD-NaOH-cpx is a pH-adjusted β CD-cpx complex and lacks the stability observed for β CD-arg-cpx.

Detectable antibiotic in the β CD-cpx complexes. The β CD-arg-cpx assemblies emitted intense blue fluorescent light that appeared along with their rod-like structures (Fig. 4a). Similar fluorescence was also observed for β CD-cpx (following the irregularly shaped structure of the complex aggregate) (Fig. 4b)

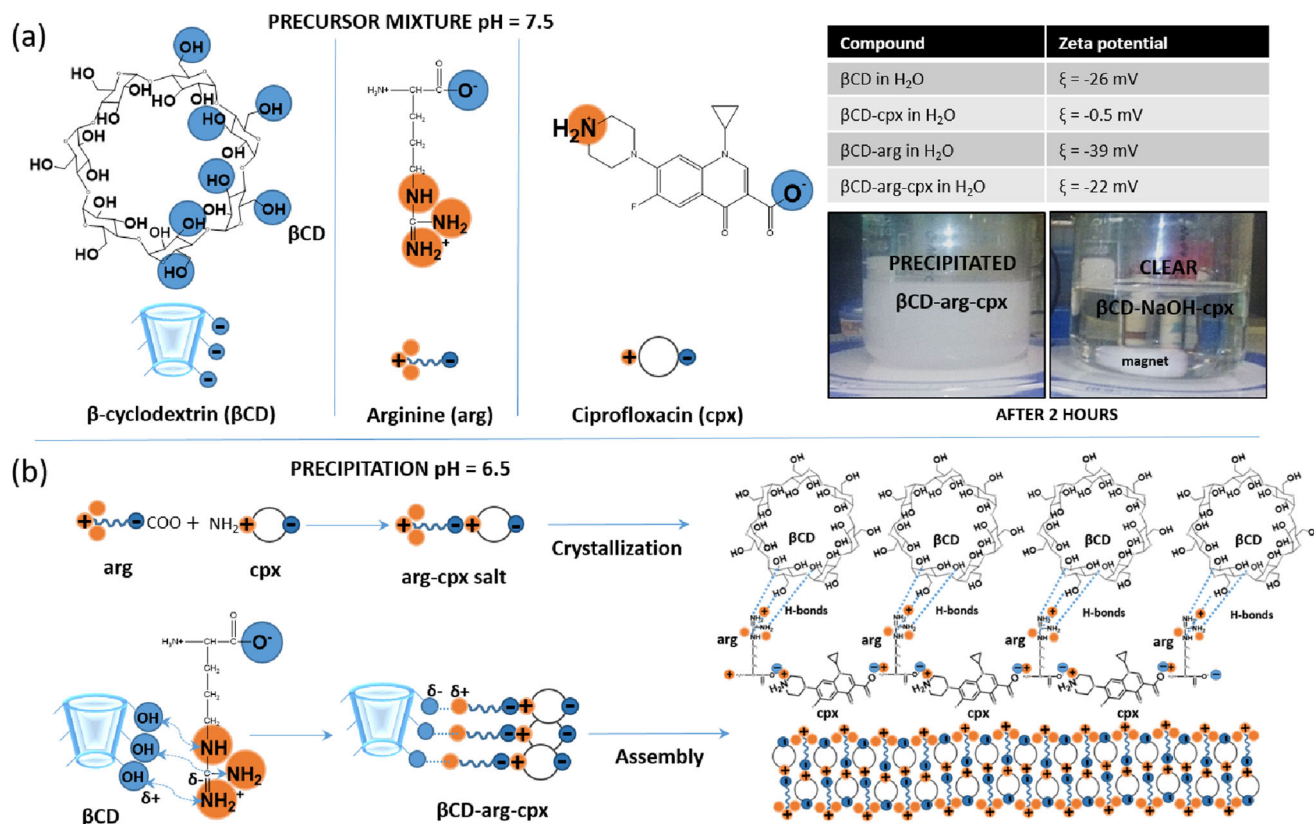


Fig. 3 Formation of more stable complex between cyclodextrin (β CD), ciprofloxacin (cpx) and arginine (arg) (β CD-arg-cpx). Molecular structures of the precursor mixture before precipitation (pH 7.5), zeta potential change for different complex components and precipitation after 2 h of mixing in the case of pH adjustment with arginine (and its delay when arg is replaced with NaOH (β CD-NaOH-cpx)) (a). Precipitation (pH 6.5) involving arg-cpx salt formation and β CD bonding followed by crystallization and assembly (b).

but not for β CD-arg (which also forms irregular aggregates) (Fig. 4c). Ciprofloxacin derivatives, in the form of spherical nanoaggregates containing perfluoroaryl and phenyl rings linked by amidine bonds to the piperazinyl group of ciprofloxacin, have been previously observed to show aggregation-induced emission (AIE)²⁷. However, to the best of our knowledge AIE in β CD-containing ciprofloxacin complexes has not been detected before.

Differences were also observed in the fluorescent spectra of β CD-arg-cpx and β CD-cpx complexes, particularly before and after dissolving in water (Fig. 4b). In solid powders, the fluorescence spectra of β CD-arg-cpx and free cpx were not the same, revealing a blueshift in the spectrum of the arginine-complexed structure. When dissolved in water, the spectrum of β CD-arg-cpx remained the same as that of the solid complex form, while the spectra of the free drug and less stable β CD-cpx inclusion complex were red-shifted with exactly the same shape of fluorescence maximum. Further analysis of the components dissolved in water revealed free cpx (and its dimers and trimers identified in MS spectra, Supplementary Fig. 5a), while in case of the β CD-arg-cpx, during aging in aqueous environment the complex released free cpx, cpx-arg, arg and β CD (Supplementary Fig. 5b).

Intensive blue fluorescence provides β CD-arg-cpx with additional detection functionality. After exposure to the β CD-arg-cpx complex for a short time, the viability of bacteria was strongly affected, as detected by the red fluorescence of propidium iodide in a high fraction of cells, which represent dead bacteria. We were also able to detect blue fluorescence from the β CD-arg-cpx rod-like assemblies, which released the complex with strong antimicrobial activity (Fig. 4c).

Complex dissolution and release. Even in a quantitative context, β CD-arg-cpx differed from the classical β CD-cpx complex (Fig. 5a). As determined from the UV-vis spectra of the remaining cpx in the solution after complex formation, β CD-arg-cpx contained three times the cpx content of β CD-cpx without arginine. The presence of arginine and its role in complex formation affected the drug content within the complex. A 1.5-fold difference in cpx content for β CD-cpx and β CD-NaOH-cpx (Fig. 5b) was observed, showing that a difference in pH did affect the content of the complex-included drug. However, in the case of β CD-arg-cpx, the effect was not solely from the contribution of pH during complex formation, since using arginine to modify the pH to the same level as for NaOH within the β CD-NaOH-cpx complex resulted in a two times higher cpx content in β CD-arg-cpx.

Along with its contribution to the formation, assembly, and incorporated drug content, arginine affected the release of the drug from the complex. In a classical inclusion β CD-cpx complex, a less stable dynamic balance between the drug and the β CD hydrophobic cone, cpx release is fast (Fig. 5b). After incubation at 37 °C in PBS buffer, more than 60% of the drug was released after 10 min of incubation. The complete decomposition of the complex and release of all the incorporated cpx took place within the first 24 h. The release kinetics were slightly slower in the case of β CD-NaOH-cpx (Fig. 5b): the initial release was approximately 40%, and at the end of 24 h, the complex released up to 70% of the incorporated drug.

In drug delivery systems (like encapsulated polymeric spheres) drug release depends on properties of the drug carrier (i.e. polymer matrix degradation, swelling, T- /pH - dependent response) which enables physical release or desorption of the

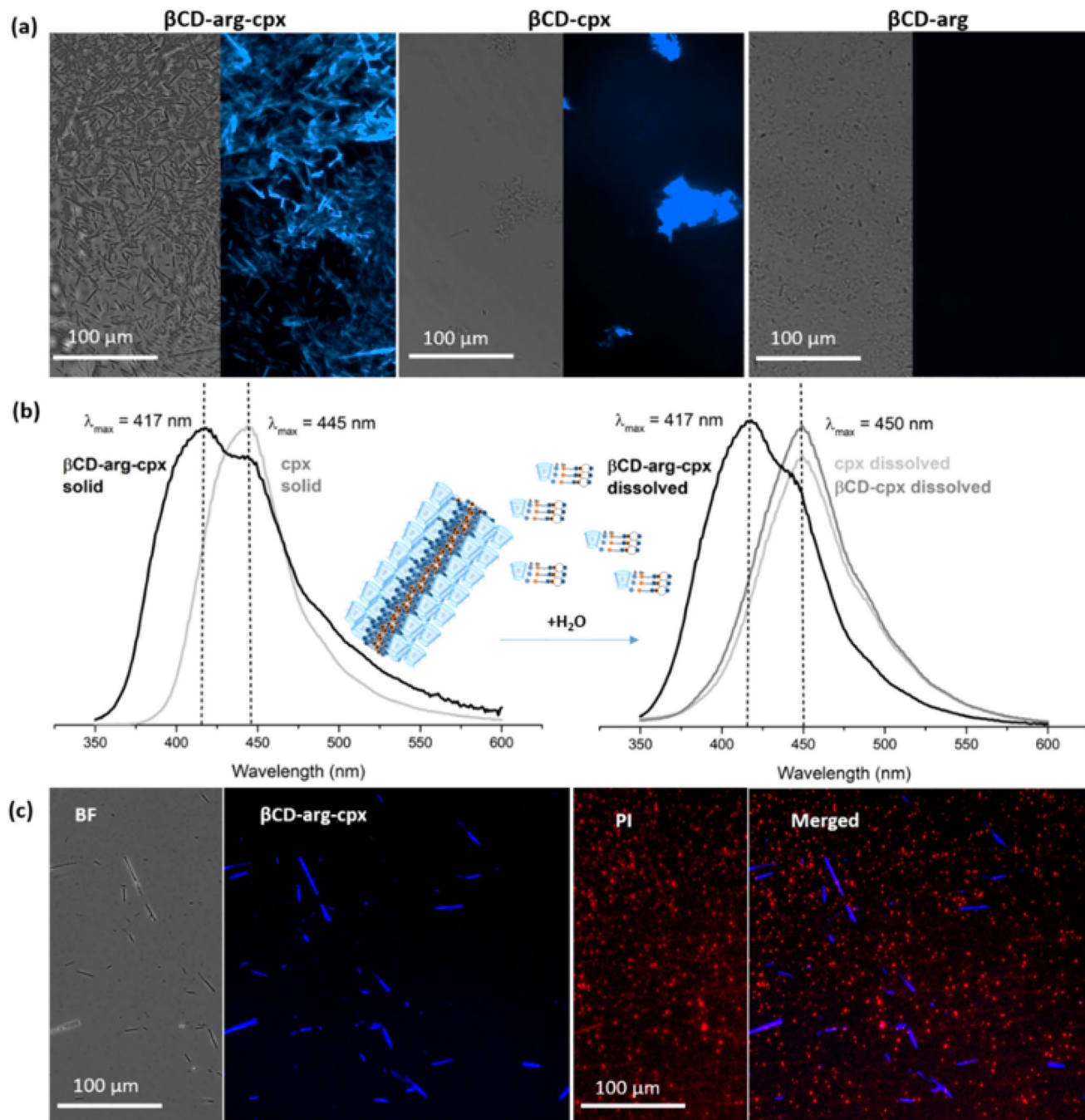


Fig. 4 Fluorescence and detection properties of the β CD-arg-Cpx complex. Blue fluorescence of cpx-containing (β CD-arg-cpx and β CD-cpx) complexes (not detected for β CD-arg) (a). Fluorescence spectra of β CD-arg-cpx and free cpx (and comparable β CD-cpx complex) before and after dissolving in water confirming different dissolving mechanisms (dissolved complex vs. dissolved free drug) (b). Detection of β CD-arg-cpx and of bacteria (100 μ g/ml of the complex after 10 min exposure to *P. aeruginosa* PAO1 stained with propidium iodide (PI, red fluorescence, detecting dead bacteria) (c).

entrapped drug. In current case the drug, as part of the complex, is a part of drug delivery system and its release depends on stability and solubility of the complex. Due to the difference in the assembly the β CD-arg-cpx complex was more stable than the inclusion complex of β CD-cpx and the pH-modified β CD-NaOH-cpx complex, showing the slowest release (Fig. 5b). Self-assembly of the natural CDs and drug complexes is known to affect their solubility¹². Initially, this complex released only 20% of the incorporated drug, and the release continued slowly, with up to 30% of the drug released after 24 h. The application of β CD as an excipient or the application of arginine to create a drug salt

within β CD-drug complexes is a convenient way to enhance drug solubility. In contrast, the novel β CD-arg-cpx complex disassembles slowly, decreases drug dissolution and enables control over drug release. The observed contribution to drug solubility is a consequence of the different bonding of the drug to the other two components (as illustrated in Fig. 3). Instead of incorporating the hydrophobic part of the drug within the β CD cone and bonding arginine to its hydrophilic part, which usually remains outside the β CD cone, the drug is bonded to the β CD surface via an arginine linker, which makes the whole structure more stable against dissolution. Moreover, the forces that hold together the

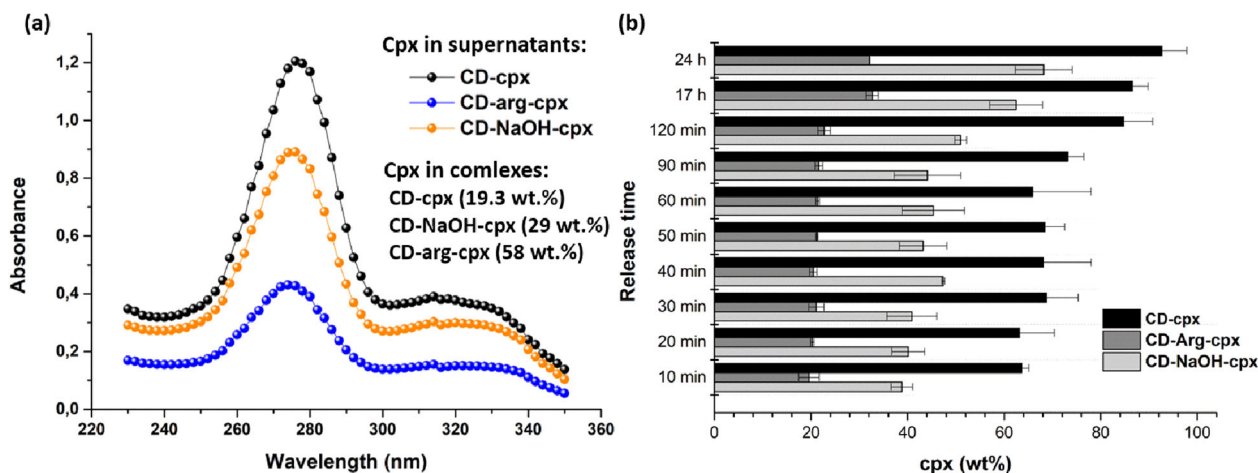


Fig. 5 Ciprofloxacin (cpx) contents in complexes and its release. Cpx in supernatants obtained after complex synthesis (and calculated contents of cpx in β CD complexes) (drug released from CD-arg-Cpx complex indicated with blue, from CD-NaOH-Cpx complex in orange and from CD-Cpx in black) (a) and comparative drug release kinetics from β CD-cpx (black), β CD-arg-cpx (dark grey) and β CD-NaOH-cpx (light grey) (b); $n = 3$; error bars refer to SD of drug release.

Table 1 Minimal inhibitory concentrations (MICs) of β CD and its complexes against gram-positive and gram-negative bacterial strains, their cytotoxicity to mammalian cells and their selectivity indices.

<i>E. coli</i>	<i>P. aeruginosa</i>	<i>S. aureus</i>	CC ₅₀ (μ M)
NA/NA	NA/NA	NA/NA	NT
NA/NA	NA/NA	NA/NA	NT
0.208/0.052 (59,615)	0.780/0.520 (5962)	0.780/0.520 (5962)	>3100
0.056/0.014 (97,143)	0.210/0.140 (9714)	0.210/0.140 (9714)	>1360
0.0045/< 0.0015 (813,333)	0.018/0.012 (101,666)	0.060/0.0049 (248,979)	1220

Minimal inhibitory concentrations (MIC) and 50% inhibitory concentrations (IC₅₀) for *Escherichia coli* (*E. coli*), *Pseudomonas aeruginosa* (*P. aeruginosa*), and *Staphylococcus aureus* (*S. aureus*). Cytotoxic concentrations (CC₅₀) were evaluated in lung epithelial A549 cells. The selectivity index (SI), calculated as CC₅₀/IC₅₀, is indicated in parentheses next to the IC₅₀. β -Cyclodextrin (β CD), 2- β -cyclodextrin-arginine (β CD-arg), 3-ciprofloxacin (cpx), 4- β -cyclodextrin-ciprofloxacin (β CD-cpx), and 5- β -cyclodextrin-arginine-ciprofloxacin (β CD-arg-cpx). NA no detected activity, NT nontoxic.

long rod-like assemblies of β CD-arg-cpx also contribute to slower disassembly and provide release control. In contrast to all of the available CD-associated platforms used to modify antibiotics, to the best of our knowledge the possibility of using arginine in creating a slowly-release antibiotic drug delivery system from β CD has not been conferred before.

In vitro antimicrobial efficacy and safety. Having observed the unconventional decreased solubility and slowed antibiotic release from the β CD-arg-cpx assembly, we next investigated of the effect of the complex in antimicrobial efficacy and toxicity testing. First, the susceptibility and minimal inhibitory concentrations (MICs) of β CD-arg-cpx and β CD-cpx complexes and their precursor components, β CD, β CD-arg, and cpx, were investigated against several bacterial strains, including gram-negative *E. coli* MG1655 (ATCC 47076) and *P. aeruginosa* PAO1 (ATCC 15692) and gram-positive *S. aureus* Rosenbach (ATCC 12600), as summarized in Table 1. None of the investigated bacterial strains showed any susceptibility to β CD or β CD-arg. For β CD-cpx, we found MIC values of 0.056 μ M for *E. coli* and 0.21 μ M for *P. aeruginosa* and *S. aureus* (Table 1). If we take into account the 19-wt% cpx content in β CD-cpx and up to 70% drug release during a 24-h incubation at 37 °C (Fig. 5b), the MICs correspond to 0.0074 μ M and 0.028 μ M free drug equivalents. Relative to the cpx reference, the β CD-cpx inclusion complex provided increases of approximately 28-fold in antimicrobial activity for all bacterial strains tested. The antibacterial efficacy of β CD-arg-cpx was higher

than those of the others with MICs of 0.0045 μ M for *E. coli*, 0.018 μ M for *P. aeruginosa* and 0.060 μ M for *S. aureus*. With 58 wt% cpx content and up to 30% drug release (Fig. 5b), the MIC was equal to 0.0008 μ M, 0.003 μ M and 0.010 μ M free cpx equivalents, respectively. Accordingly, compared to the cpx reference, β CD-arg-cpx had 260-fold, 260-fold and 78-fold increased antimicrobial activity for the bacterial strains tested, respectively.

Cytotoxicity in mammalian cells was evaluated using lung epithelial cells (A549) (Table 1 and Fig. 6a). The β CD-arg-cpx complex was characterized as nontoxic (with a high CC₅₀ value of 2000 μ g/ml (1220 μ M)). Only high-concentration doses (>1000 μ g/ml (611 μ M)) of β CD-arg-cpx showed a dose-dependent reduction in cell viability (Fig. 6b), which corresponded to approximately 100,000–800,000 times higher MICs. The complexation of cpx to β CD decreases the toxicity (Table 1). Furthermore, it is important to note that the selectivity index (SI) increased in the different bacterial tests compared to that of soluble cpx (13 times for *E. coli*, 17 times for *P. aeruginosa*, and 42 times for *S. aureus*) (Table 1). In other words, while nanomolar concentrations exhibited efficient antimicrobial activity, millimolar concentrations were needed for toxic effects, presenting an extensive therapeutic window for safe application of the complex and increasing the possible in vivo efficacy compared to soluble commercial cpx.

We next investigated the antimicrobial activity by analyzing MIC values and kinetics in bacterial growth, as presented in Fig. 6b for the case of *P. aeruginosa*. More details on microdilution test performed for β CD-arg-cpx and β CD-cpx

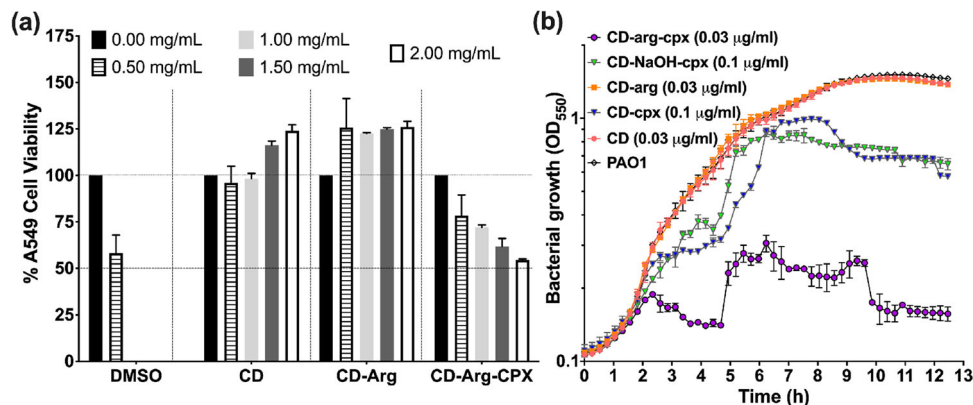


Fig. 6 Antimicrobial properties vs. cytotoxicity of CD complexes. Cytotoxicity of β CD-arg-cpx and its components to lung epithelial A549 cells (a). The plot shows the percentage of A549 cell viability after incubation with different concentrations of β CD complexes (0 mg/ml (black), 0.5 mg/ml (patterned), 1 mg/ml (light grey), 1.5 mg/ml (dark grey) and 2 mg/ml (black border)). DMSO was used as a positive control for toxicity, while untreated A549 monolayers were used as a negative control for cytotoxicity; $n = 3$; error bars refer to SD of viability relative to non-treated cells. Comparison of *P. aeruginosa* PAO1 growth (white) in the presence of β CD-arg-cpx (0.03 μ g/ml or 0.020 μ M) (purple), β CD-NaOH-cpx (0.2 μ g/ml or 0.132 μ M) (green), β CD-cpx (0.2 μ g/ml or 0.140 μ M) (blue), β CD-arg (0.03 μ g/ml or 0.0023 μ M) (orange) and β CD (0.03 μ g/ml or 0.0026 μ M) (rose) (b); $n = 3$; error bars refer to optical density SD.

complexes, CD-arg and CD auxiliary components as well as direct comparison of the β CD-arg-cpx to free cpx drug are presented in Supplementary Fig. 6. The complex components, β CD, and β CD-arg did not alter bacterial growth. On the other hand, at 0.2 μ g/ml, both β CD-cpx and β CD-NaOH-cpx (as β CD-cpx version obtained in alkaline medium) (with 0.140 μ M and 0.132 μ M molar concentrations, respectively) slowed bacterial growth with clear bacteriostatic effects, while β CD-arg-cpx enabled bactericidal effects at 0.03 μ g/ml (0.018 μ M). These results provided clear evidence that the improvement in antimicrobial activity for β CD-arg-cpx is not a consequence of the pH at which the complex is formed (although β CD-NaOH and β CD-arg-cpx have similar structures). Moreover, it directly reflects the special role of arginine as a linker. The decrease in MIC between the classical less stable β CD-cpx inclusion complex and more stable β CD-arg-cpx assembly may be a consequence of how they release and disassemble. Due to weak interactions between antibiotics and β CD in the inclusion complex, when they dissolve, the complex decomposes, enabling the release of the free drug. On the other hand, when arginine connects β CD and cpx, the binding forces are stronger, and disassembling the rod-like structures results in a gradual release of free cpx and also cpx-arg as more active drug form.

In a morphological context, after cpx and β CD-arg-cpx treatment of gram-negative bacteria (*E. coli* and *P. aeruginosa*), we observed bacterial filamentation (Figs. 7 and 8, respectively). This was an evidence that the primary antibacterial mechanism of cpx was not changed, and it was also observed when the drug was within the β CD-arg-cpx complex assembly. Cpx is well known to affect DNA replication by targeting DNA gyrase, which inhibits bacterial cell division^{30,31}. Under antibiotic-induced stress, bacteria that stop cell division continue their growth by inhibiting cell septation, increasing their length, and forming long filaments³². Depending on the stress conditions, bacteria inside filaments can survive or die³⁰. If individual cell units connected within a filament remain viable and form long multicellular chains, stress relief occurs in the evolving antibiotic-resistant strain³¹. In that context, subinhibitory concentrations of cpx induce the filamentation of rod-shaped bacteria as a transition step toward their evolution into cpx-resistant strains³². After treatment with very low, subinhibitory cpx concentrations, 0.003 μ g/ml (0.008 μ M) in *E. coli* and 0.03 μ g/ml (0.08 μ M) in *P. aeruginosa*, we observed very intensive and long filamentation

in *E. coli* (Fig. 7b, e, h) (compare to non-treated reference (Fig. 7a, d, g), while *P. aeruginosa* showed only cell elongation with few cases of very long filaments (Fig. 8b, e, h) (which was not detected in reference (Fig. 8a, d, g)). Connected division septa, observed in SEM images, resulted from bacterial inhibition of cell division. Only some filamented cells were dead, as revealed by live/dead staining, while the majority remained alive and survived the stress induced by the low concentration of cpx (Figs. 7e, 8e). The bacterial cell membrane remained intact (as shown by staining with FM464 only at the surface) and clearly showed several nucleosomes along the filaments (stained with DAPI) (Figs. 7h, 8h). We also observed normal-sized bacteria connected to the ends of the filaments (Fig. 7h), indicating debugging and the possible formation of antibiotic-resistant strains.

A completely different situation was seen when treating at the same concentrations of the β CD-arg-cpx complex used for soluble cpx (Figs. 7, 8). In *E. coli*, a very low cpx concentration (0.003 μ g/ml (0.002 μ M) of the β CD-arg-cpx complex effectively stopped bacterial growth and decreased the number of filamented cells (Fig. 7c). The filaments contained intact cell membranes and multinucleosome entities (Fig. 7i). Most importantly, all of the detected bacteria, normal-sized and filamented, were confirmed to be dead (Fig. 7f). A similar result was obtained for *P. aeruginosa* exposed to a low cpx concentration (0.03 μ g/ml (0.02 μ M)) of the β CD-arg-cpx complex. Although the number of formed filaments increased, a closer look at their surface revealed strong damage, while their environment showed many cell fragments remaining after decomposition (Fig. 8c). Similar decomposition of *P. aeruginosa* was detected after exposure to a high cpx dose (0.2 μ g/ml (0.52 μ M), which resulted in increased membrane vesicle formation induced by an explosive cell lysis mechanism³⁰. As observed in *E. coli*, all the filamented *P. aeruginosa* were dead (Fig. 8f). FM464/DAPI revealed their multinuclear structure and membrane deformation into vesicles (Fig. 8i). Deformation of the membrane, vesicle formation, and cellular damage by explosive cellular lysis were progressive and depended on the β CD-arg-cpx complex concentration (Supplementary Fig. 7). At lower concentrations (0.03 μ g/ml (0.02 μ M)), both filaments and normal-sized cells were detected. They all had damaged cell walls containing small holes and were partially decomposed into vesicles (200 nm in size). At a higher β CD-arg-cpx concentration (0.1 μ g/ml (0.06 μ M)), filaments were no longer detected, and all of the remaining normal-sized cells were

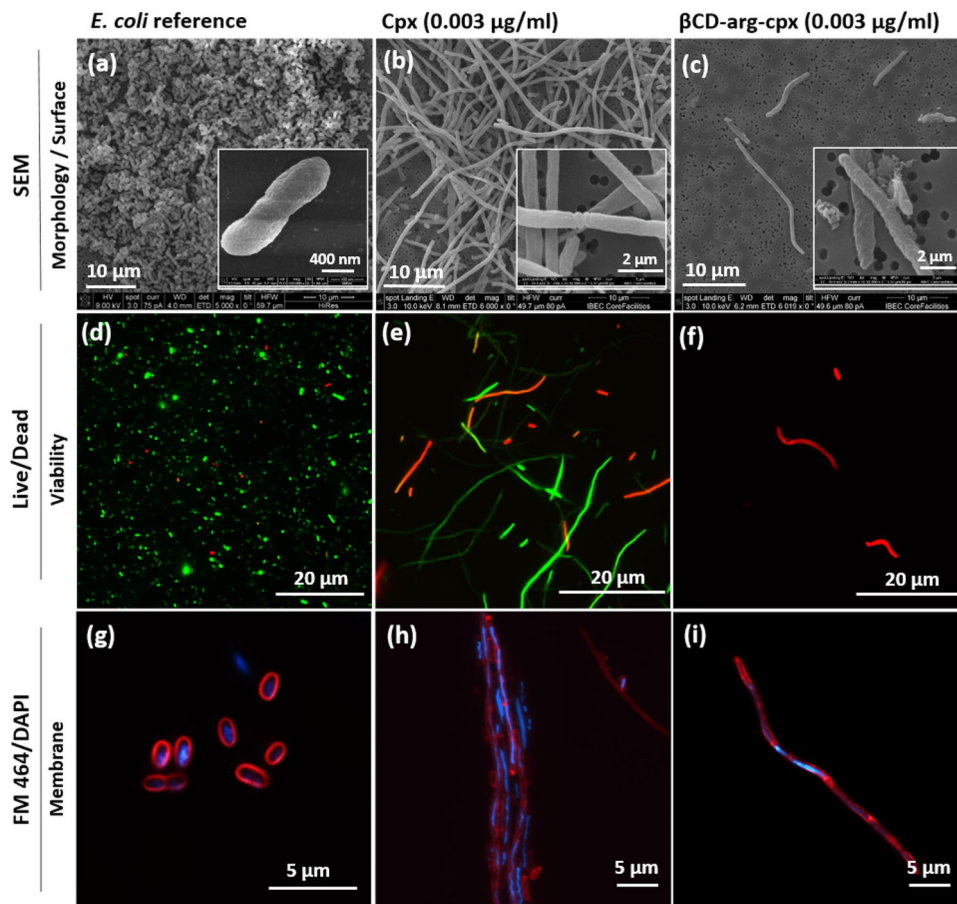


Fig. 7 *E. coli* MG1655 exposed to ciprofloxacin and the βCD-arg-cpx complex. Morphology and surface of *E. coli* cells before (a) and after exposure to low cpx concentration (0.003 µg/ml or 0.008 µM) (b) and equivalent of cpx in βCD-arg-cpx (0.003 µg/ml or 0.002 µM) (c); Live *E. coli* stained with a Live/Dead dyes (d) and fraction of viable *E. coli* cells treated with 0.003 µg/ml (0.008 µM) cpx (e) and βCD-arg-cpx (0.002 µM) (f). Membrane structure of wild-type *E. coli* stained with FM464/DAPI dyes (g) and bacteria treated with 0.003 µg/ml pure cpx (0.008 µM) (h) and CD-arg-cpx complex (0.002 µM) (i).

completely lysed into vesicle-like cell wall fragments approximately 100 nm in size. Progressive cell damage indicated their response to the increasing stress induced by the cpx loaded in the complex. Similar changes including intensive deformations in the membrane, damage to the structure of the cells, and finally antimicrobial activity when the βCD-arg-cpx complex was used at much lower concentrations than the free cpx drug were also observed for *S. aureus*, a gram-positive strain (Supplementary Fig. 8).

In vivo antimicrobial efficacy and safety. The in vivo toxicity and efficacy of the βCD-arg-cpx complex were investigated in *Galleria mellonella* worms (Fig. 9) as an animal model previously optimized to evaluate antibacterial efficacy and toxicology^{33,34}. Toxicity was investigated at high concentrations of the complex (up to 2421 mg/kg), and 100% survival was observed for all of the investigated concentrations. For the antibacterial efficacy study, worms were preinfected with *P. aeruginosa* PAO1³⁵. Without any treatment, 100% death was obtained after 24 h. Postinfection treatment with βCD-arg-cpx at concentrations of 5 mg/kg (3.3 mM) and 10 mg/kg (6.6 M) resulted in 100% survival. As a reference, treatment with 5 mg/ml (13.3 mM) free cpx resulted in only 20% survival. Better efficacy of treatment with the βCD-arg-cpx complex in comparison with the free drug is further supported by the fact that the complex contains only 58 wt% cpx,

which is slowly released from the assembled structures (as shown in Fig. 5).

The basic underlying mechanism of antimicrobial action in the assembled βCD-arg-cpx complexed drug remains the same as that of its free form drug. The βCD-arg-cpx complex has the same ability to inhibit cellular division progress typically obtained with free cpx as well as to induce similar stress-related changes in bacteria, such as filamentation and explosive lysis driven by membrane vesicle formation. Although these two drug forms use the same mechanism of action, a difference in their efficacy is evident and could be attributed to a difference in their bioavailability. The presence of the βCD component, with the known ability to increase interactions with cell wall components¹², certainly promotes drug transfer through the membranes and consequently increases the antimicrobial efficacy at available concentrations inside the bacterial cell. However, as has been seen after direct comparison of less stable βCD-arg inclusion and more stable βCD-arg-cpx complexes, the effect cannot be attributed solely to the presence of βCD. Due to the reversible nature of bonding in inclusion complexes, solubilization provides the free drug form in balance with βCD molecules. This type of balance enhances drug transfer across the membrane but is far less effective as more stable βCD-arg-cpx complex form. More stable βCD-arg-cpx, in which βCD and cpx are bonded via an arginine linker, enables βCD to act as a building component of the drug molecule. Along with βCD, the transfer of the drug

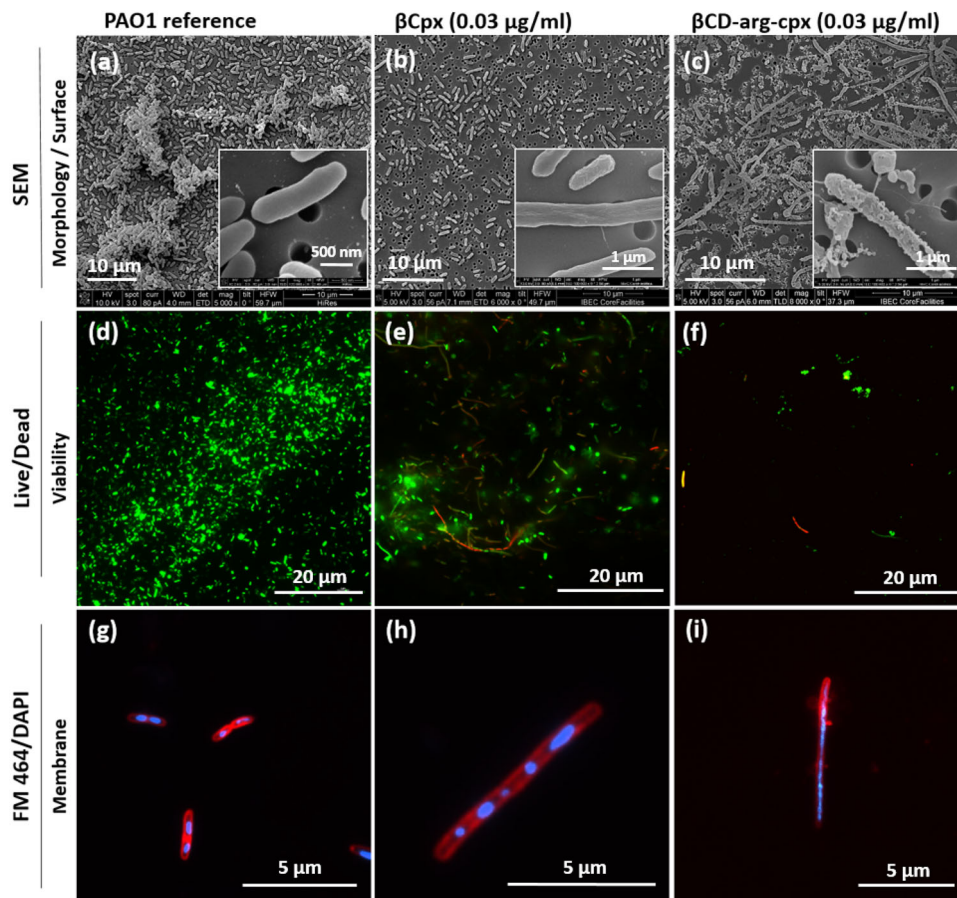


Fig. 8 *P. aeruginosa* PAO1 exposed to ciprofloxacin and its β CD-arg complex. Morphology and surface of PAO1 cells before (a) and after exposure to low cpx concentration (0.03 μ g/ml or 0.08 μ M) (b) and equivalent cpx in β CD-arg-cpx (0.03 μ g/ml or 0.02 μ M) (c). Live *P. aeruginosa* PAO1 stained with a Live/Dead dyes (d) and fraction of viable cells treated with 0.03 μ g/ml cpx (0.08 μ M) (e) and β CD-arg-cpx (0.02 μ M) (f). Membrane structure of wild-type *P. aeruginosa* PAO1 stained with FM464/DAPI dyes (g) and bacteria treated with 0.03 μ g/ml pure cpx (0.08 μ M) (h) and β CD-arg-cpx complex (0.02 μ M) (i).

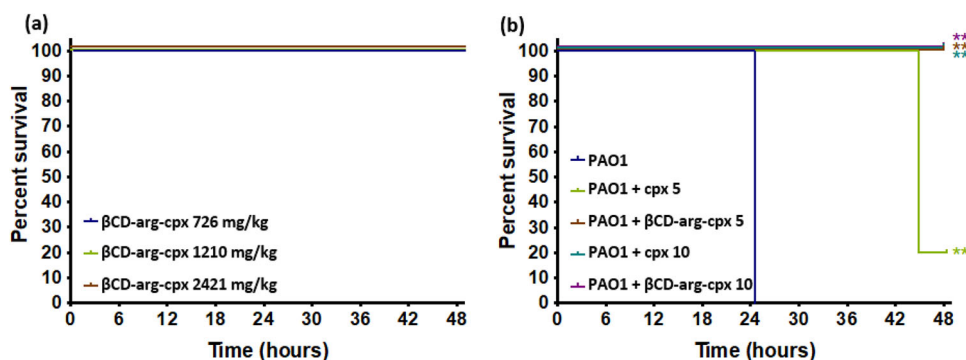


Fig. 9 Kaplan-Meier survival curves for in vivo toxicity and efficacy in the *Galleria mellonella* larva model. Toxicity of β CD-arg-cpx complex showing very high larval survival for the whole concentration range tested (up to 2421 mg/kg) (a). Comparative antibacterial efficacy study in larvae infected with PAO1 (dark blue) and treated with the β CD-arg-cpx complex (light green and brown) and free cpx drug (dark green and purple) (equivalent cpx content of 5 and 10 mg cpx/kg larva, respectively) that shows higher survival of the preinfected worms after treatment with the complex (b). Asterisks: statistically significant differences versus *P. aeruginosa* PAO1 control in a log-rank test (** p value < 0.01); $n = 5$. This figure represents the same experiment repeated several times, which yielded identical results every time.

through the membrane is also affected by the presence of arginine and its bonding to drug molecule.

Consequently, complexed cpx was more effectively transferred to its target (DNA gyrase) and was able to induce the same level of stress as much higher concentrations of free cpx. If the complex concentrations were high enough (still much lower than

the effective concentrations of free drug), the interactions of β CD and arginine bonded to the drug with bacterial wall components were sufficient to disintegrate the bacterial cell structure and induce an explosive lysis process. All these facts indicate that stress induced at very low concentrations of β CD-arg-cpx, enables an important enhancement in antimicrobial activity. Detailed

investigations of the potential of the complexed drug form to prevent adaptive evolutionary processes that produce resistant strains remains as interesting challenge for the future.

Conclusion

This innovative type of β CD complexes, in which linkers are used to make more stable connections between β CD and a drug, hold potential for enhancing the efficacy of previously approved, clinically used antibiotics. Produced using very simple, technologically non-demanding, and highly economical chemistry, such complexes could be very promising tools for repurposing, reprofiling, or reusing different drugs. Future research in this area should be focused on exploring all of the available possibilities introduced by enhancing drug bioavailability within this type of complex, including their capacity to develop and affect antibiotic-resistant strains, mitigate drug toxicity, and enhance biocompatibility. Such complexes can offer additional options in antibiotic pipeline and encourage the pharmaceutical industry to explore more effective forms of old antibiotics and to actively participate in resolving the global lack of effective antibiotics as a persistent and very serious health problem in the modern era.

Methods

Materials. The complex was formed using L-arginine (arg, L-2-amino-5-guanidinopentanoic acid, C₁₆H₁₄N₄O₂, Sigma-Aldrich, Germany), ciprofloxacin-hydrochloride (cpx, Cayman Chemical Company) and β -cyclodextrin (β CD, Sigma-Aldrich C4805, Germany). All the chemicals and reagents used were of analytical grade. All of the experiments were performed using laboratory-produced undistilled water.

β CD-arg-cpx complex synthesis. Before forming the complex, arginine (50 ml, 0.4 mg/ml) and cyclodextrin (50 ml, 2 mg/ml) were dissolved in water with continuous stirring (200 rpm) for 15 h at room temperature. The premixed solutions were added to aqueous ciprofloxacin solution (0.8 mg/ml), and stirring (200 rpm) was continued for the next 24 h. The white precipitate appeared 2 h after ciprofloxacin addition. After 24 h of mixing, the supernatant was separated by centrifugation (8000 rpm), and the precipitate was redispersed in 5 ml of distilled water. The dispersion was frozen in dry ice (for 3 h) and freeze-dried (24 h, Christ Alpha 1-4, Martin Christ). Control samples were formed following the same protocol but with replacement of arginine with a water solution of NaOH to form β CD-NaOH-cpx and with replacement of arginine with distilled water to form β CD-cpx. Due to a lack of precipitation in control samples, the total volume of the mixture was frozen and freeze-dried. All powders were kept in covered glass containers and stored under ambient conditions for further testing.

Physicochemical characterization. Powder X-ray diffraction analyses (pXRD) were performed in the 2–70° 2 θ range with a 0.02° step size and 2 s per step recording using a Bruker AXS D4 Endeavor diffractometer. Fourier transform infrared spectroscopic (FTIR) investigations were performed by a Perkin Elmer Spectrum 400 MIR spectrophotometer using the DRIFT technique. Spectra were recorded in powders obtained by mixing 5 mg of samples with 80 mg of KBr. X-ray photoelectron spectroscopy (XPS) was performed with the Versaprobe 3 AD (Phi, Chanhassen, US) using monochromatic Al-K α X-ray source. For each measurement, spectra were acquired on a 200 μ m spot size with the charge neutralizer turned on, as the pellets were put on a non-conductive double tape. Survey spectra were measured at 280 eV pass energy and step of 1 eV, while high-resolution spectra were measured at 27 eV pass energy and step of 0.025 eV. Charge neutralization was used, so the energy scale of XPS spectra were corrected with shifting C1s peak of carbon to binding energy of 284.8 eV. XPS data were analysed with PHI Multipak software. In order to remove surface layer of the pellet to examine underlying surface, sputtering of the sample with argon clusters was used. Sample was sputtered for 1 min at 5 kV and 20 nA over 2 \times 2 mm area, followed by 200 μ m high-resolution point analysis. Dissolution products were identified using mass spectrometry. Measurements were performed using a hybrid orthogonal acceleration time-of-flight mass spectrometer Q-ToF PremierTM (Waters-Micromass, Manchester, U.K.) equipped with atmospheric pressure ionization (API) sources and coupled with an ultra-performance liquid chromatograph (TOF MS/UpLC). The detection was performed via an electrospray ionization (ESI) source in positive mode. For morphological scanning electron microscopy (SEM, Nova NanoSEM), powders were dispersed in water and deposited on 50-nm filter membranes stuck on carbon tape and coated with 5 nm carbon. Structural transmission electron microscopy analyses (TEM, Tecnai Spirit 120 kV) were performed on samples dispersed in water and deposited on copper grids. STEM images were taken with Verios 4 G HP (Thermo Fisher Scientific, Waltham, Massachusetts, USA) scanning

electron microscope (SEM) in STEM mode. Energy-Dispersive X-ray Spectroscopy (EDXS) system with Ultim Max 65 detector and AZtec software (Oxford Instruments Abingdon, United Kingdom) was used for the EDS mapping. Fluorescence imaging was performed on water-dispersed powders dropped on microscope slides using a Nikon inverted fluorescence microscope ECLIPSE Ti-S/L100 (Nikon) coupled with a DS-Qi2 Nikon camera. Zeta potentials were measured using a Mavern Nanosizer.

Antimicrobial tests. Antibacterial testing was performed using *Escherichia coli* MG1655 (ATCC 47076), *Pseudomonas aeruginosa* PAO1 (ATCC 15692), and *Staphylococcus aureus* Rosenbach (ATCC 12600). The strains were cultured overnight at 37 °C in liquid growth medium (Luria Bertani, LB) (Scharlab, Spain) for *E. coli* and *P. aeruginosa* and tryptic soy broth (TSB) (Scharlab, Spain) for *S. aureus*. Bacterial samples were ultrasonically dispersed in growth medium for 30 s (A = 18%, W = 250 W, on:off = 2:1 s) to form 2 mg/ml stocks, which were further diluted to the tested concentrations. Microtiter plate wells (96-well assay plate, tissue culture-treated polystyrene; Costar 3595, Corning Inc., Corning, NY) were inoculated with 100 μ l of bacteria (OD₅₅₀ = 0.05) and 100 μ l of the specific serial dilutions of the tested samples. Controls included growth medium and bacteria without treatment. Incubation was performed in an Infinite M200 Pro multimode microplate reader (Tecan) at 37 °C for 14 h with continuous orbital shaking. Bacterial growth was assessed by measuring optical density at 550 nm every 15 min. All concentrations were tested repeatedly in three replicates ($n = 3$).

Live/Dead study in bacteria. To assess bacterial viability, the tested samples were dispersed in LB or TSB growth medium for 30 s (A = 18%, W = 250 W, on:off = 2:1 s) and mixed with bacteria to a final volume of 1 ml (OD₅₅₀ = 0.3). After incubation for 12 h, 100 μ l was centrifuged for 5 min at 6000 rpm, and the supernatant was replaced with 25 μ l of Live/Dead BacLight Bacterial Viability Test (Invitrogen, Thermo Fisher Scientific) containing SYTO9 and propidium iodide (PI) in 1X phosphate-buffered saline (PBS) at a 1:1 ratio and a concentration of 3 \times 10⁻⁶ mg/ml. It was followed by a 15-min incubation in the dark to stain the bacteria. Fluorescent bacteria were visualized by a Nikon inverted fluorescence microscope ECLIPSE Ti-S/L100 (Nikon) coupled with a DS-Qi2 Nikon camera (Nikon).

FM 464/DAPI study in bacteria. To assess membrane integrity, the tested samples were dispersed in LB or TSB growth medium for 30 s (A = 18%, W = 250 W, on:off = 2:1 s) and mixed with bacteria to a final volume of 1 ml (OD₅₅₀ = 0.3). After incubation for 12 h, 100 μ l was centrifuged for 5 min at 6000 rpm, and the supernatant was replaced with 50 μ l of FM 464 (N-(3-triethylammonium propyl)-4-(6-(4-(diethylamino)phenyl)hexatrienyl)pyridinium dibromide, Invitrogen, Thermo Fisher Scientific)/DAPI (diamidino-2-phenylindole (DAPI; Biotium, Fremont, CA) in Hank's balanced salt solution (HBSS) (containing 0.4 μ l of 5 mg ml⁻¹ FM 464 and 1 μ l of 125x DAPI). Samples were stained for 15 min in ice, light protected, and subsequently analyzed using a Nikon fluorescent ECLIPSE Ti-S/L100 microscope.

Scanning electron microscopy study in bacteria. Morphological analyses of bacterial cells affected by the investigated complex were performed using FEISEM (Nova NanoSEM). One hundred microliters of bacteria incubated with the complex for 12 h was centrifuged for 5 min at 6000 rpm and fixed after replacing the growth medium with 50 μ l of glutaraldehyde (3 wt %). The fixation step was performed for 3 h at room temperature. Fixed bacteria were deposited on porous membranes by filtration under soft vacuum, washed three times with PBS (for 15 min for each wash), and dehydrated in serially diluted ethanol (30, 50, 70, 90, and 100 wt %, 30 min at each concentration). The samples were dried at critical points.

In vitro toxicity study. Testing was performed in human lung epithelial A549 cells (ATCC® CCL-185™). Cells were cultured in DMEM/F-12 (Gibco, Thermo Fisher Scientific) supplemented with 1% (v/v) penicillin-streptomycin (Gibco, Thermo Fisher Scientific) and 10% (v/v) decomplexed fetal bovine serum (Gibco, Thermo Fisher Scientific) and grown in a humidified incubator (Mettmert) at 37 °C and 5% (v/v) CO₂. The tested complex was ultrasonically dispersed in DMEM for 30 s (A = 18%, W = 250 W, on:off = 2:1 s) to form a stock solution (2 mg/ml). Cells grown to confluence in a 96-well plate were treated with serial dilutions of the complex and incubated at 37 °C in 5% CO₂ for 24 h. The cytotoxicity assay was performed by adding 20 μ l of 10 \times Presto blue™ Cell Viability Reagent (Molecular Probes, Invitrogen, Thermo-Fisher Scientific) per well, incubating for 30 min and recording fluorescence at excitation $\lambda = 560$ nm and emission $\lambda = 590$ nm. The references included the complex without cells in DMEM, the pure dye in DMEM, cells without the complex (as a negative control), and cells with DMSO (as a positive control). All concentrations were tested repeatedly in triplicate ($n = 3$). Viability has been normalized to cells without treatment (viability % to negative control).

In vivo toxicity. *Galleria mellonella* larvae, used as an in vivo model³⁵, were grown at 34 °C until a 200–250 mg weight. The investigated complex was dispersed in PBS during the toxicity study using ultrasound (30 s, A = 18%, W = 250 W, on:off = 2:1 s) to form a 5 mg/ml stock solution. A 10 µl inoculum of the complex dispersion (in different concentrations) was injected into the upper right proleg area of the larvae using a Hamilton 22-gauge syringe. Each concentration of the complex was injected into five larvae per testing group ($n = 5$). The control group was inoculated with 10 µl of 1x PBS (Fisher Scientific) in the same manner. After inoculation, the larvae were kept at 37 °C for up to 72 h. Larval mortality was observed every 16–24 h. The testing was done repeatedly. The survival curves were plotted using Kaplan–Meier analysis, and statistically significant differences were determined by the one-sided log-rank test (GraphPad 9.0 Software).

In vivo antibacterial efficacy. During the efficacy study, *G. mellonella* larvae were preinjected with 10 µl of an infective dose of *P. aeruginosa* (PAO1) (6.4×10^3 cfu/ml) in the upper right proleg area. An hour after infection, a 10 µl inoculum containing different concentrations of the tested complex dispersed in PBS was injected into the upper left proleg. The following procedure was the same as for the toxicity study. The controls were larvae injected with 1x PBS (negative control) and larvae injected with ciprofloxacin (without complex) at 10 mg/kg (positive control). Each group tested contained five larvae ($n = 5$).

Statistics and reproducibility. The experiments were done at least in triplicate and repeated 2–3 times (depend on the experiment). Results are presented as mean value \pm SD. Differences between groups were assessed by the one-sided log-rank test (GraphPad 9.0 Software).

Reporting summary. Further information on research design is available in the Nature Research Reporting Summary linked to this article.

Data availability

All data generated or analyzed during this study are included in this published article and its supplementary information files. The source files behind Figs. 2, 4, 5, 6 and 9 are presented in Supplementary Data 1–5 files, respectively. The source files behind Supplementary Figs. 1–4 and 6 are provided in Supplementary Data 6–10 files, respectively.

Received: 12 May 2022; Accepted: 31 October 2022;

Published online: 12 November 2022

References

1. The world is running out of antibiotics, WHO report confirms, *World Health Organization (WHO) Report* <https://www.who.int/news/item/20-09-2017-the-world-is-running-out-of-antibiotics-who-report-confirms> (2019).
2. Plackett, B. No money for new drugs. *Nature* **586**, S50–S53 (2020).
3. Farha, M. A. & Brown, E. D. Drug repurposing for antimicrobial discovery. *Nat. Microbiol.* **4**, 565–577 (2019).
4. Guy, R. K., DiPaola, R. S., Romanelli, F. & Dutch, R. E. Rapid repurposing of drugs for COVID-19. *Science* **368**, 829–830 (2020).
5. Zhou, Y., Wang, F., Tang, J., Nussinov, R. & Cheng, F. Artificial intelligence in COVID-19 drug repurposing. *Lancet Digit. Health* **2**, e667–e676 (2020).
6. Talevi, A. & Bellera, C. L. Challenges and opportunities with drug repurposing: finding strategies to find alternative uses of therapeutics. *Expert Opin. Drug Discov.* **15**, 397–401 (2020).
7. Agrawal, P. Advantages and challenges in drug re-profiling. *Pharmacovigil* **S2**, e002 (2015).
8. Naylor, S., Kauppi, D. M. & Schonfeld, J. P. Therapeutic drug repurposing, repositioning and rescue part II: overview. *Drug Discov. World* **16**, 57–72 (2015).
9. Brown, D. Antibiotic resistance breakers: can repurposed drugs fill the antibiotic discovery void? *Nat. Rev.* **14**, 821–832 (2015).
10. Theuretzbacher, U., Outtersson, K., Engel, A. & Karlén, A. The global preclinical antibacterial pipeline. *Nat. Rev.* **18**, 275–285 (2020).
11. Wong, C. E., Dolzhenko, A. V., Lee, S. M. & Young, D. J. Cyclodextrins: a weapon in the fight against antimicrobial resistance. *J. Molec. Eng. Mater.* **5**, 1740006 (2017).
12. Saokham, P., Muankaew, C., Jansook, P. & Loftsson, T. Solubility of cyclodextrins and drug/cyclodextrin complexes. *Molecules* **23**, 1161 (2018).
13. Uekama, K., Hirayama, F. & Irie, T. Cyclodextrin drug carrier systems. *Chem. Rev.* **98**, 2045–2076 (1998).
14. Nardello-Rataj, V. & Leclercq, L. Encapsulation of biocides by cyclodextrins: toward synergistic effects against pathogens. *Beilstein J. Org. Chem.* **10**, 2603–2622 (2014).

15. Redenti, E., Szente, L. & Szejtli, J. Cyclodextrin complexes of salts of acidic drugs. Thermodynamic properties, structural features, and pharmaceutical applications. *J. Pharm. Sci.* **90**, 979–986 (2001).
16. Mura, P. et al. Solid-state characterization and dissolution properties of naproxen–arginine–hydroxypropyl- β -cyclodextrin ternary system. *Eur. J. Pharm. Biopharm.* **59**, 99–106 (2005).
17. Sherje, A. P., Patel, F., Murahari, M., Suvarna, V. & Patel, K. Study on effect of L-arginine on solubility and dissolution of Zaltoprofen: preparation and characterization of binary and ternary cyclodextrin inclusion complexes. *Chem. Phys. Lett.* **694**, 120–128 (2018).
18. Mennini, N., Maestrelli, F., Cirri, M. & Mura, P. Analysis of physicochemical properties of ternary systems of oxapropazolin with randomly methylated- β -cyclodextrin and L-arginine aimed to improve the drug solubility. *J. Pharm. Biomed. Anal.* **129**, 350–358 (2016).
19. Sapte, S. & Pore, Y. Inclusion complexes of cefuroximeaxetil with β -cyclodextrin: physicochemical characterization, molecular modeling and effect of L-arginine on complexation. *J. Pharm. Anal.* **6**, 300–306 (2016).
20. Rincón-Ortiz, S. A., Botero, M. A. & Ospina, R. XPS characterization of ciprofloxacin tablet. *Surf. Sci. Spectra* **29**, 014020 (2022).
21. Al-Omar, M. A. Ciprofloxacin: physical profile. *Profiles Drug Subst. Excip.* **31**, 163–178 (2004).
22. Sambasevam, K. P., Mohamad, S., Sarih, N. M. & Ismail, N. A. Synthesis and Characterization of the Inclusion Complex of β -cyclodextrin and Azomethine. *Int. J. Mol. Sci.* **14**, 3671–3682 (2013).
23. Kacso, I., Borodi, G., Fărcaș, S. I. & Bratu, I. Inclusion compound of vitamin B13 in β -cyclodextrin. structural investigations. *J. Phys.: Conf. Ser.* **182**, 012009 (2009).
24. Sosa, L. V. et al. The structure, molecular dynamics, and energetics of Centrin–Melittin complex. *Proteins* **79**, 3132–3143 (2011).
25. Bhongade, B., Talath, S. & Dhaneshwar, S. A validated method for the quantitation of ciprofloxacin hydrochloride using diffuse reflectance infrared fourier transform spectroscopy. *Int. J. Spectrosc. ID* **2014**, 294612 (2014).
26. Mesallati, H., Umerska, A., Paluch, K. J. & Tajber, L. Amorphous polymeric drug salts as ionic solid dispersion forms of ciprofloxacin. *Mol. Pharmaceutics* **14**, 2209–2223 (2017).
27. Xie, S. et al. Design and synthesis of theranostic antibiotic nanodrugs that display enhanced antibacterial activity and luminescence. *Proc. Natl Acad. Sci. USA* **114**, 8464–8469 (2017).
28. Neves, M. A. C., Yeager, M. & Abagyan, R. Unusual arginine formations in protein function and assembly: rings, strings, and stacks. *J. Phys. Chem. B* **116**, 7006–7013 (2012).
29. Zhang, F., Gu, S., Ding, Y., Zhang, Z. & Li, L. A novel sensor based on electropolymerization of β -cyclodextrin and L-arginine on carbon paste electrode for determination of fluoroquinolones. *Anal. Chem. Acta* **770**, 53–61 (2013).
30. Hooper, D. C. Mechanisms of fluoroquinolone resistance. *Drug Resist. Updat.* **2**, 38–55 (1999).
31. Bos, J. et al. Emergence of antibiotic resistance from multinucleated bacterial filaments. *PNAS* **112**, 178–183 (2015).
32. Turnbull, L. et al. Explosive cell lysis as a mechanism for the biogenesis of bacterial membrane vesicles and biofilms. *Nat. Comm.* **7**, 11220 (2016).
33. Moya-Anderico, L. et al. Utility of *Galleria mellonella* larvae for evaluating nanoparticle toxicology. *Chemosphere* **266**, 129235 (2021).
34. Blanco-Cabra, N. et al. Novel oleoic and maslinic acid derivatives as a promising treatment against bacterial biofilm in nosocomial infections: an in vitro and in vivo study. *ACS Infect. Dis.* **5**, 1581–1589 (2019).
35. Moya-Anderico, L., Admella, J., Fernandes, R. & Torrents, E. Monitoring gene expression during a *Galleria mellonella* bacterial infection. *Microorganisms* **8**, 1798 (2020).

Acknowledgements

The authors are grateful to Angel Blanco Blanes and Dr. Samuel Sanchez from the Smart Nano-Bio-Devices group at the Institute for Bioengineering of Catalonia for zeta potential measurements as well as to Dr Dušan Žigon from Center for Mass Spectrometry at Jozef Stefan Institute for ToF MS analysis. The European Commission has funded this work under Horizon 2020's Marie Skłodowska-Curie Actions COFUND scheme (Grant Agreement no. 712754) and by the Severo Ochoa program of the Spanish Ministry of Science and Competitiveness (Grant SEV-2014-0425 (2015-2019)). E.T. was supported by grants from the Spanish Ministerio de Economía y Competitividad (MINECO/FEDER) (RTI2018-098573-B-I00), Generalitat de Catalunya (2017SGR-1079 and CERCA program), the Catalan Cystic Fibrosis associations and the La Caixa Foundation. Additional funding support has been provided to M.V. by grants from the Slovenian Research Agency (ARRS) (grants J2-8169, N2-0150, and P2-0091).

Author contributions

M.V. research concept, synthesis and characterization, writing first draft; L.G. XRD and FTIR analyses, M.K. TEM and EDS analyses, J.H. STEM and elemental mapping analysis,

B.J. XPS analysis, L.M.-A. in vivo study, M.C. in vitro toxicity, E.T. mentoring and funding. All authors contributed to editing text to final version.

Competing interests

The authors declare no competing interests.

Additional information

Supplementary information The online version contains supplementary material available at <https://doi.org/10.1038/s42003-022-04197-9>.

Correspondence and requests for materials should be addressed to Marija Vukomanovic or Eduard Torrents.

Peer review information *Communications Biology* thanks John-Sigurd Svendsen and the other, anonymous, reviewer(s) for their contribution to the peer review of this work. Primary Handling Editor: Christina Karlsson Rosenthal.

Reprints and permission information is available at <http://www.nature.com/reprints>

Publisher's note Springer Nature remains neutral with regard to jurisdictional claims in published maps and institutional affiliations.



Open Access This article is licensed under a Creative Commons Attribution 4.0 International License, which permits use, sharing, adaptation, distribution and reproduction in any medium or format, as long as you give appropriate credit to the original author(s) and the source, provide a link to the Creative Commons license, and indicate if changes were made. The images or other third party material in this article are included in the article's Creative Commons license, unless indicated otherwise in a credit line to the material. If material is not included in the article's Creative Commons license and your intended use is not permitted by statutory regulation or exceeds the permitted use, you will need to obtain permission directly from the copyright holder. To view a copy of this license, visit <http://creativecommons.org/licenses/by/4.0/>.

© The Author(s) 2022

Supplementary Information

Development of a ternary Cyclodextrin–Arginine–Ciprofloxacin antimicrobial complex with enhanced stability

M. Vukomanovic^{1,2,*}, L. Gazvoda^{1,2}, M. Kurtjak¹, J. Hrescak,³ B. Jaklic,^{1,2} L. Moya-Andérico⁴, M. Cendra⁴, E. Torrents^{4,5,*}

¹Advanced Materials Department, Institute Jozef Stefan, Jamova 39, Ljubljana, Slovenia

²International Postgraduate School of Jozef Stefan, Jamova 39, Ljubljana, Slovenia

³Center for Electronic Microscopy and Microanalysis (CEMM), Institute Jozef Stefan, Jamova 39, Ljubljana, Slovenia

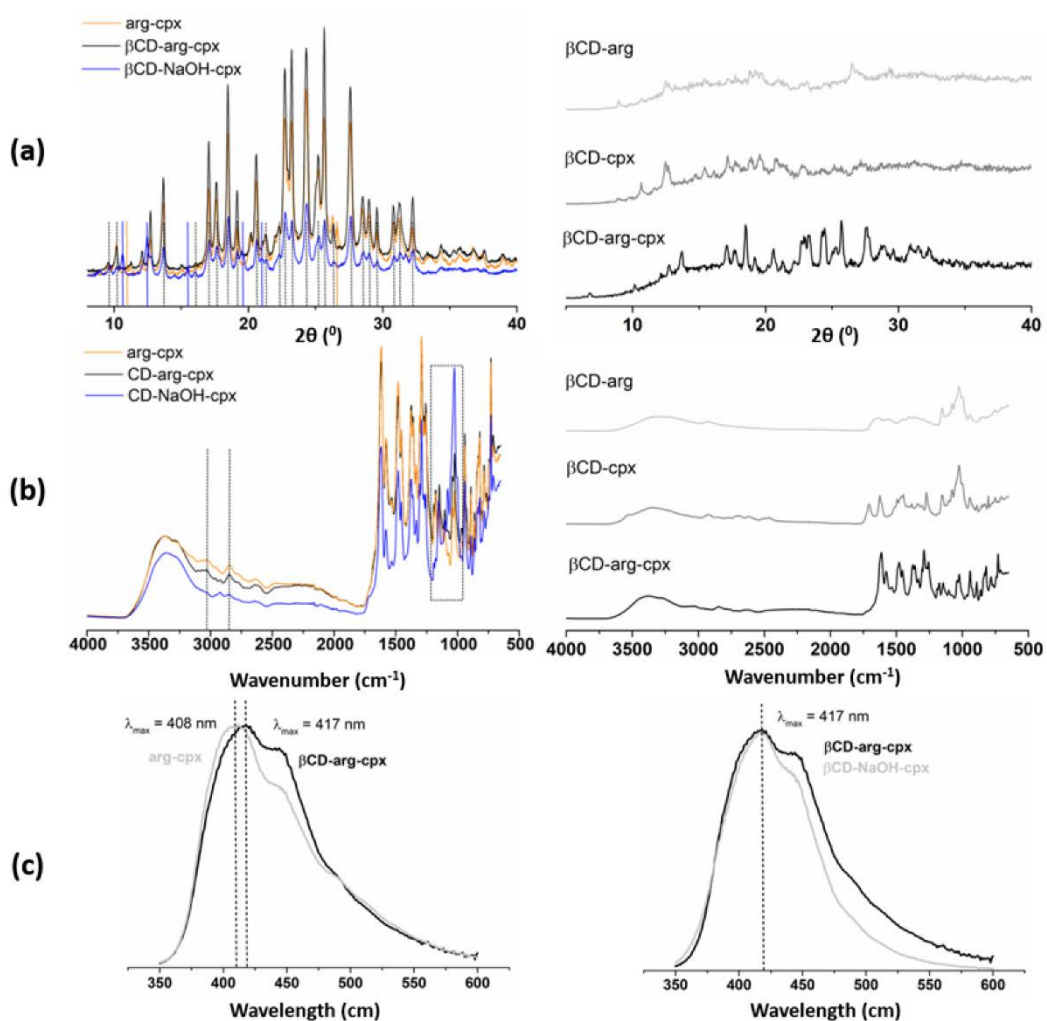
⁴Bacterial Infections: Antimicrobial Therapies, Institute for Bioengineering of Catalonia (IBEC), The Institute of Science and Technology, Baldori Reixac 15-21, 08028 Barcelona, Spain

⁵Microbiology Section, Department of Genetics, Microbiology and Statistics, Faculty of Biology, University of Barcelona, 643 Diagonal Ave., 08028, Barcelona, Spain

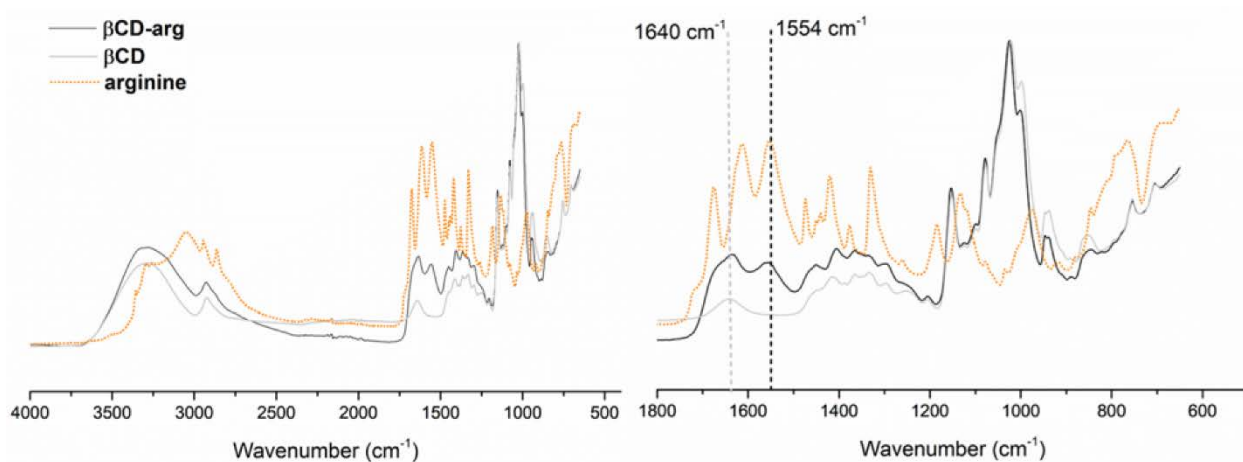
*Corresponding authors:

Dr. Eduard Torrents: etorrents@ibecbarcelona.eu

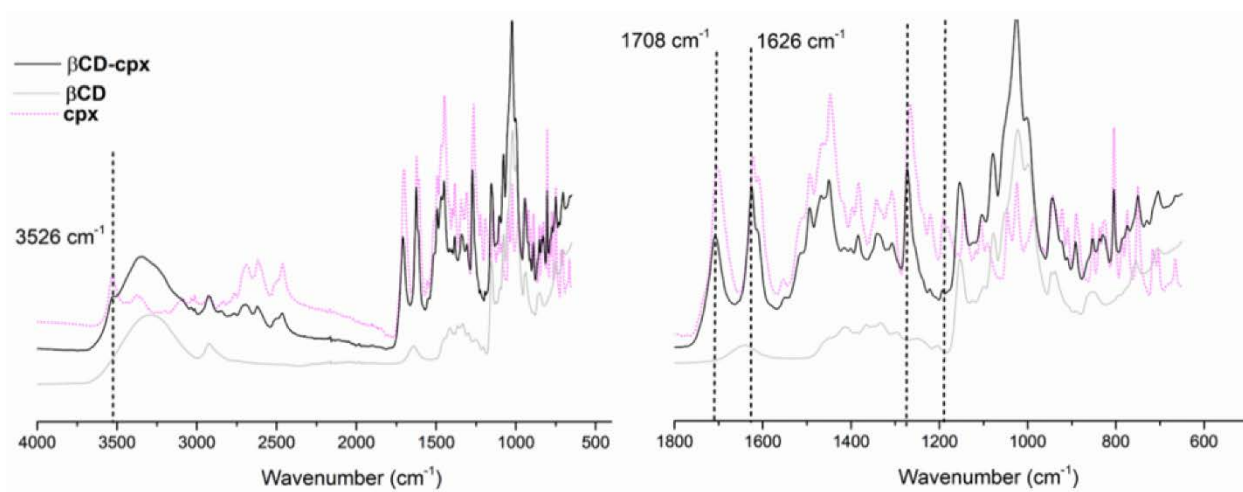
Dr. Marija Vukomanovic: marija.vukomanovic@ijs.si



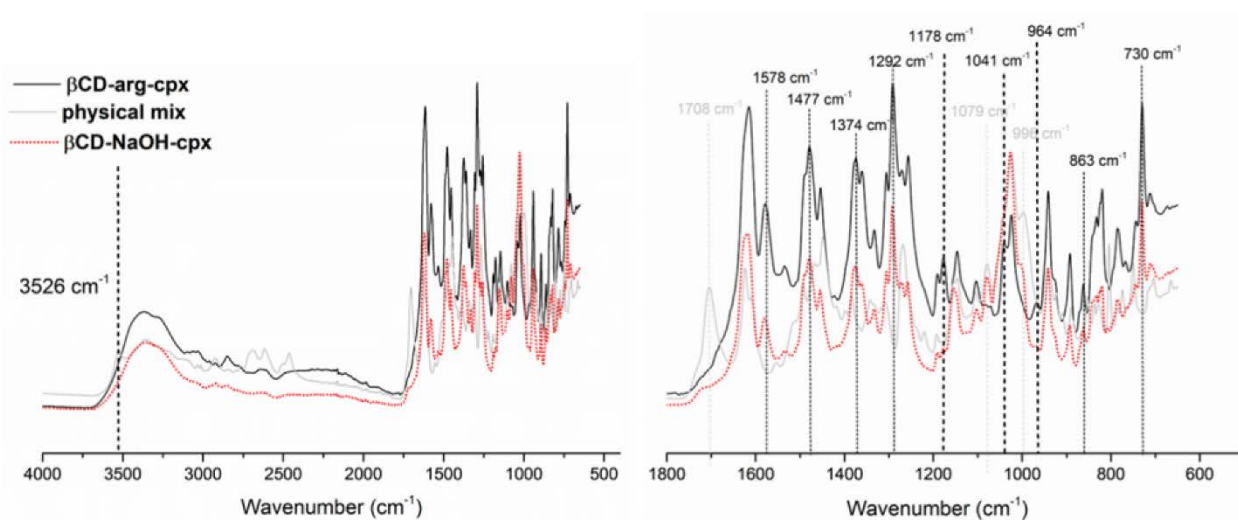
Supplementary Figure 1. Structural and chemical properties of CD-based complexes. Very similar crystal structures of arg-cpx, β CD-arg-cpx, and β CD-NaOH-cpx detected by XRD and their differences compared to β CD-arg and β CD-cpx (a). FTIR spectra showing differences in functional group vibrations in arg-cpx, β CD-arg-cpx, and β CD-NaOH-cpx, as well as their components (β CD-arg and β CD-cpx) (b). Position shifts detected in fluorescence spectra of cpx in complexes with and without β CD as well as the absence of the change in the case of cpx deprotonation with arg or NaOH (c).



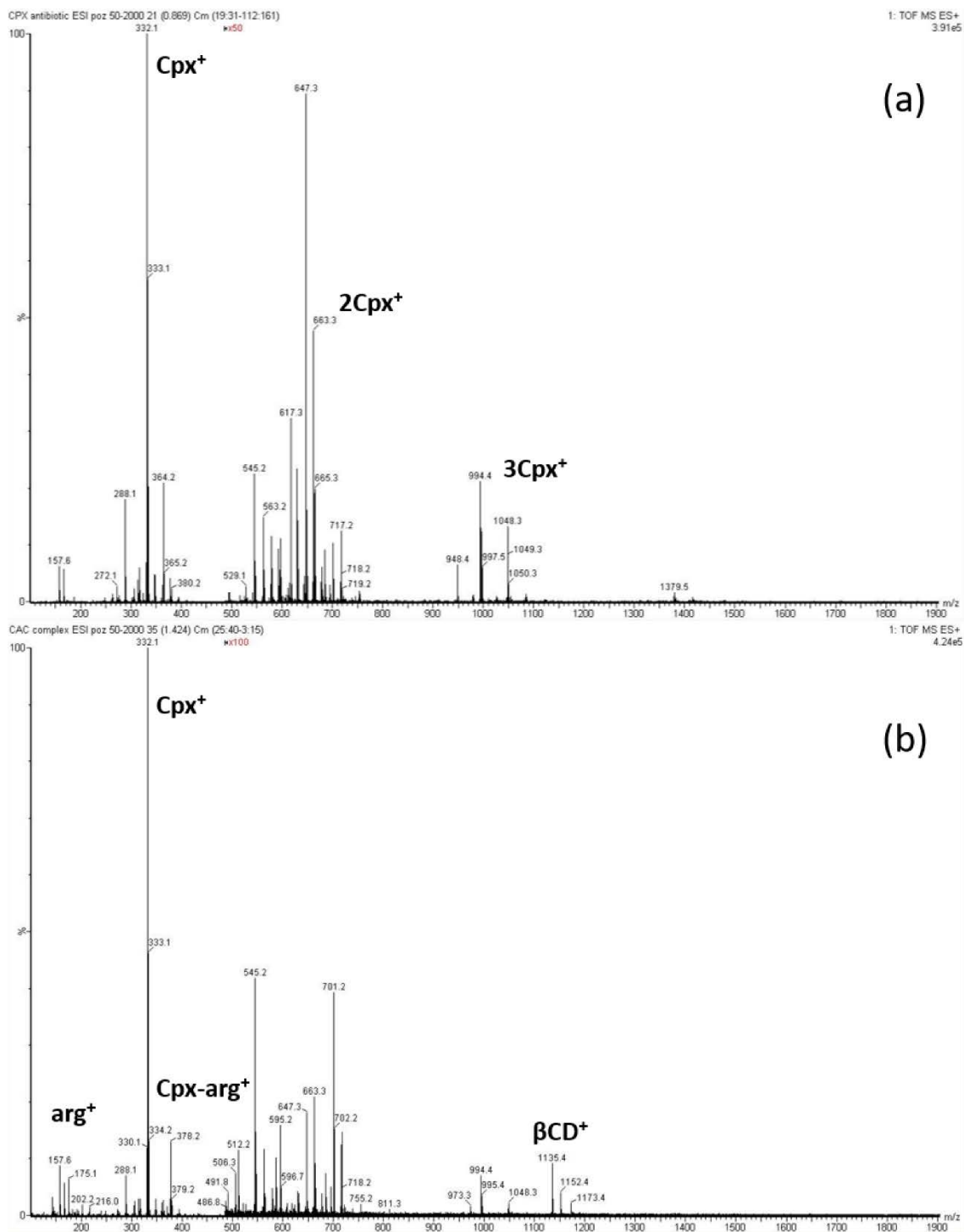
Supplementary Figure 2. FTIR spectra of the β CD-arg complex and its components arginine (arg) and cyclodextrin (β CD); annotated bands from β CD and arg components with increasing intensity within the complex.



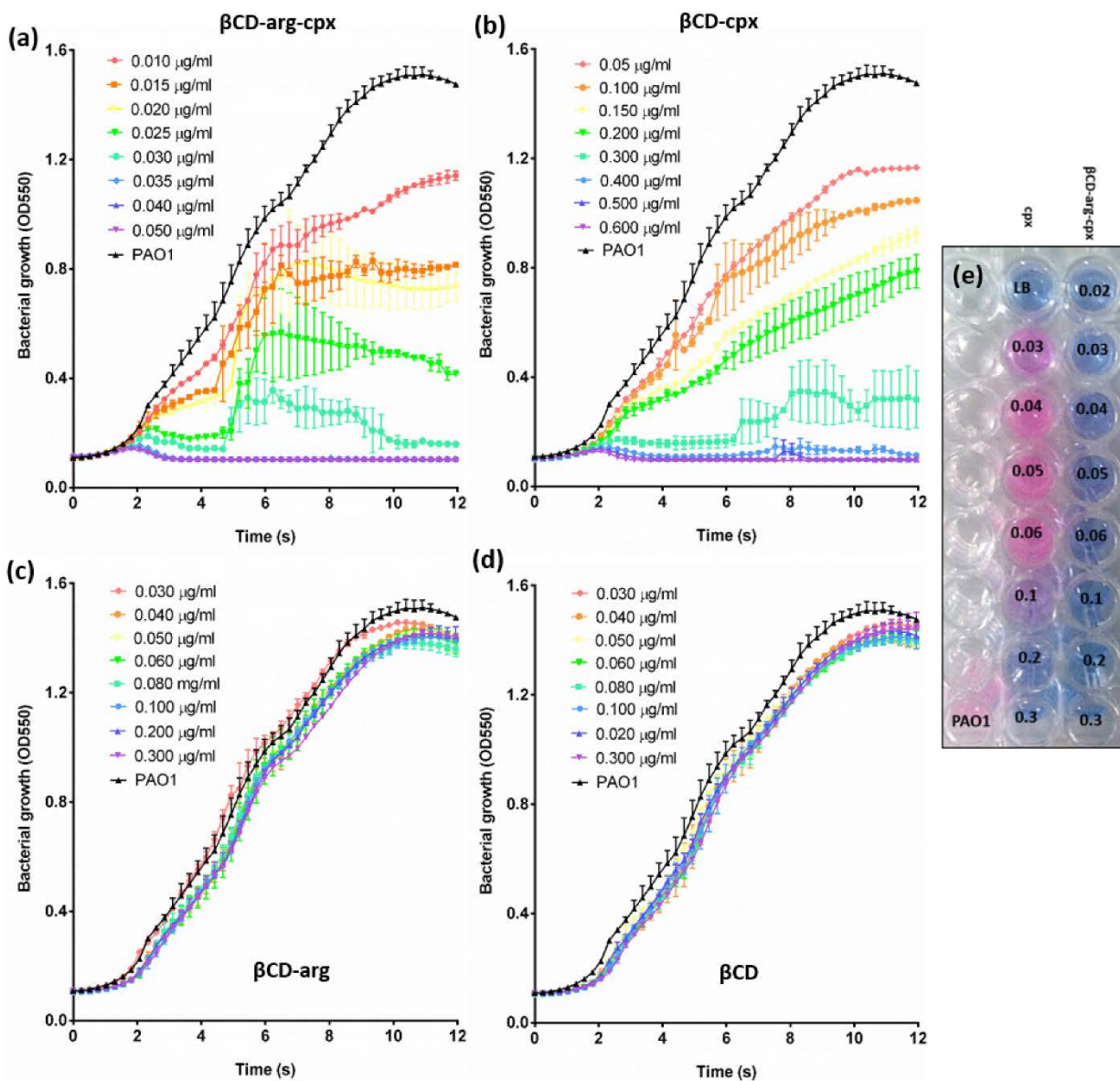
Supplementary Figure 3. FTIR spectra of the CD-cpx inclusion complex and its components ciprofloxacin (cpx) and cyclodextrin (CD); annotated bands of OH vibrations that also remain within the complex (absence of intermolecular hydrogen bonding) and shifts of the bands after complex formation due to interactions after incorporating cpx inside the CD cone.



Supplementary Figure 4. FTIR spectra of β CD-arg-cpx more stable complex (with arginine linker), β CD-NaOH-cpx complex (with arginine replaced by NaOH), and physical mixture of complex components; bands of OH vibrations that disappear in complexed structures (due to deprotonation of a carboxyl group), novel vibrations (marked in black vertical dashed lines), and suppressed vibrations (marked in gray vertical lines) observed after β CD-arg-cpx and β CD-NaOH-cpx complex formation are annotated. Bold black dashed lines annotate bands characteristic of β CD-arg-cpx that do not exist in the β CD-NaOH-cpx spectrum, identifying differences in their structures.

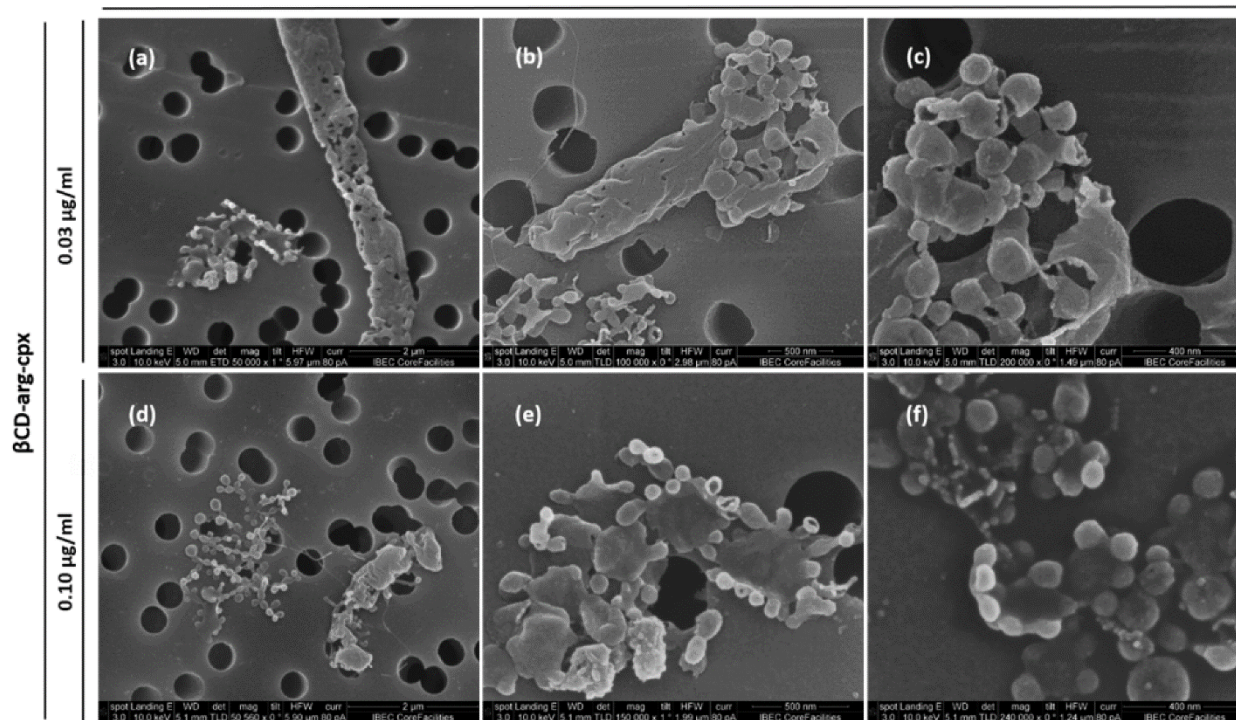


Supplementary Figure 5. Mass spectra of components released in water after complete dissolving cpx (a) and partial dissolving of βCD-arg-cpx complex (b) during 24-h aging in aqueous environment.

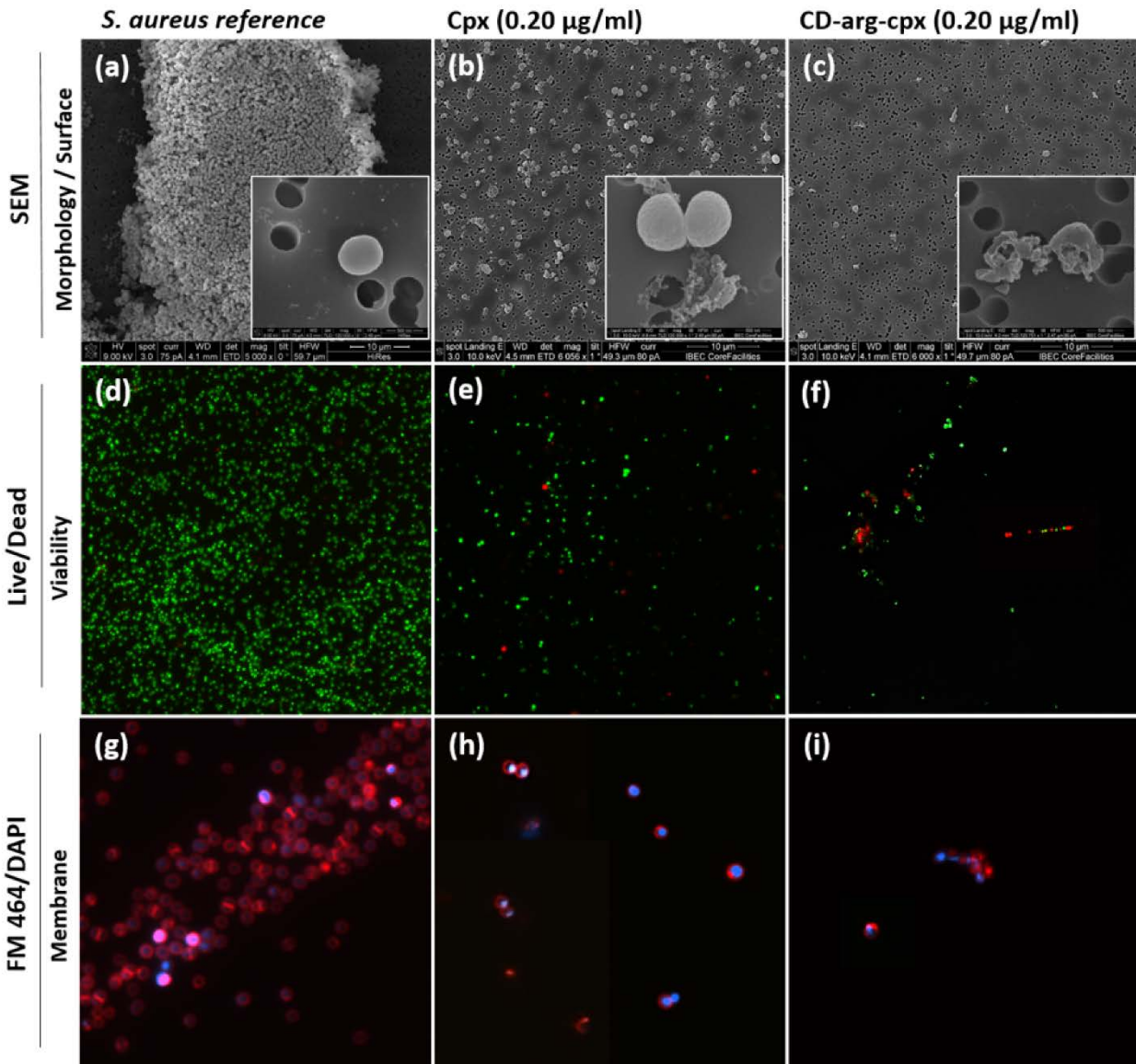


Supplementary Figure 6. Microdilution test showing kinetics of PAO1 growth in presence of β CD-arg-cpx (0.010-0.050 μ g/ml) (a), β CD-cpx (0.050-0.60 μ g/ml) (b), β CD-arg (0.030-0.300 μ g/ml) (c) and β CD (0.030-0.300 μ g/ml) (d) as well as Presto blue test showing direct comparison between activity of β CD-arg-cpx and free cpx drug (e); n=3, error bars refer to CD of optical density.

PAO1



Supplementary Figure 7. Decomposition of membrane into vesicle-like structures observed in *P. aeruginosa* PAO1 for filamented and normal-sized cells (β CD-arg-cpx concentration 0.03 μ g/ml (0.02 μ M)) (a-c) and only nonfilamented bacteria (β CD-arg-cpx concentration 0.1 μ g/ml (0.06 μ M)) (d-f).



Supplementary Figure 8. *S. aureus* exposed to ciprofloxacin and its β CD-arg complex. Morphology and surface of *S. aureus* before (a) and after exposure to low cpx concentration (0.20 $\mu\text{g}/\text{ml}$) (b) and equivalent cpx in β CD-arg-cpx (c) cells; live *S. aureus* stained with Live/Dead dyes (d) and fraction of viable cells treated with 0.03 $\mu\text{g}/\text{ml}$ cpx (e) and β CD-arg-cpx (f); membrane structure of wild-type *S. aureus* stained with FM464/DAPI dyes (g) and in bacteria treated with 0.03 $\mu\text{g}/\text{ml}$ of cpx (h) and β CD-arg-cpx complex (i).